1 **The mitochondrial phosphate carrier *Tb*MCP11 is essential for mitochondrial function in**
2 **the procyclic form of *Trypanosoma brucei***
3
4 Fei Gao[1#], Frank Voncken[2#] Claudia Colasante[3]
5 [1] Department of Neuroscience, University of Cambridge, Cambridge Biomedical Campus, Hills
6 Road, Cambridge, CB2 0AH, United Kingdom
7 [2] Department of Biomedical Sciences, School of Life Sciences, University of Hull, Cottingham
8 Road, Hull, HU6 7RX, United Kingdom
9 [3] Institute for Anatomy and Cell Biology, Division of Medical Cell Biology, Aulweg 123,
10 University of Giessen, 35392 Giessen, Germany
11
12 [#] These authors contributed equally to the paper
13
14

Abstract

Conserved amongst all eukaryotes is a family of mitochondrial carrier proteins (SLC25A) responsible for the import of various solutes across the inner mitochondrial membrane. We previously reported that the human parasite *Trypanosoma brucei* possesses 26 SLC25A proteins (*Tb*MCPs) amongst which two, *Tb*MCP11 and *Tb*MCP8, were predicted to function as phosphate importers. The transport of inorganic phosphate into the mitochondrion is a prerequisite to drive ATP synthesis by substrate level and oxidative phosphorylation and thus crucial for cell viability. In this paper we describe the functional characterization of *Tb*MCP11. In procyclic form *T. brucei*, the RNAi of *Tb*MCP11 blocked ATP synthesis on mitochondrial substrates, caused a drop of the mitochondrial oxygen consumption and drastically reduced cell viability. The functional complementation in yeast and mitochondrial swelling experiments suggested a role for *Tb*MCP11 as inorganic phosphate carrier. Interestingly, procyclic form *T. brucei* cells in which *Tb*MCP11 was depleted displayed an inability to either replicate or divide the kinetoplast DNA, which resulted in a severe cytokinesis defect.

32 **Introduction**

33 *Trypanosoma brucei* is the causative agent of African sleeping sickness [1] and belongs to the
34 class of the kinetoplastea as part of the subphylum Glycomonada of the Euglenozoa [2]. They
35 are characterized by the presence of specialized peroxisomes (glycosomes) and of one single
36 large mitochondrion containing circular DNA (kinetoplast DNA, kDNA) [3–7]. Like
37 mitochondria of other eukaryotes, those of *T. brucei* possess an outer permeable and an inner
38 impermeable membrane, contain DNA and compartmentalize a large number of critical
39 metabolic processes [8]. Protein mass spectrometry of *T. brucei* mitochondria revealed the
40 presence of a large array of proteins functioning in respiration, solute transport, amino acid and
41 lipid metabolism, mRNA editing and DNA and protein processing [9–11].

42 One of the most important function of mitochondria is the provision of ATP through substrate
43 level and oxidative phosphorylation, which requires the import of ADP and inorganic phosphate
44 (Pi) across the inner mitochondrial membrane [8,12,13]. The transport of these molecules is
45 facilitated by two proteins belonging to the mitochondrial carrier protein family (MCP family,
46 SLC25A family) [14–17], namely the ATP/ADP carrier (*Tb*MCP5, [18,19]) and the phosphate
47 carrier [15,20–22]. The mitochondrial ATP/ADP carrier exchanges ATP produced in the
48 mitochondrial matrix for cytosolic ADP, while the phosphate carrier replenishes the consumed
49 intramitochondrial Pi pool either in exchange with OH^- or in symport with protons [21,22].

50 Together with the mitochondrial ATP/ADP carrier and the ATP synthase, the phosphate carrier
51 forms the "ATP synthasome" [23] and is therefore indispensable for the mitochondrial ATP
52 synthesis. In the yeast *Saccharomyces cerevisiae*, depletion of the phosphate carrier resulted in
53 a reduced growth on non-fermentable carbon sources and in a reduction of the mitochondrial
54 membrane potential with concomitant inhibition of the mitochondrial protein import [24]. In
55 mammals, two isoforms (A and B) of the phosphate carrier *SLC25A3* exist that arise by
56 alternative splicing: isoform A is predominantly found in heart and skeletal muscle while isoform

57 B is ubiquitously found in all tissues [25,26]. In humans and mice, mutations in the *SLC25A3*
58 gene caused severe defects in mitochondrial metabolism and morphology, and has been
59 associated with hypertrophic cardiomyopathy [27,28].
60 One particularity of *T. brucei* is that in the two replicative stages, the procyclic form (PCF) in
61 the insect vector and the bloodstream form (BSF) in the mammalian host, ATP provision occurs
62 in different ways: the PCF generates ATP within the mitochondrion by substrate level and
63 oxidative phosphorylation through the TCA cycle and the electron transport chain, while the
64 BSF relies on glycolysis for its ATP supply [5,29–33]. This implicates differences in the function
65 of the mitochondrial phosphate carrier in the two replicative life stages of *T. brucei*.
66 We previously identified two genes, e.g. *Tb*MCP8 and *Tb*MCP11, belonging to the MCP family
67 and coding for putative phosphate carriers that might be indispensable for mitochondrial ATP
68 synthesis and viability in *T. brucei* [15]. The results we present here show that only *Tb*MCP11
69 but not *Tb*MCP8 is expressed in both BSF and PCF and that *Tb*MCP11 is indispensable to sustain
70 growth, cytokinesis and the mitochondrial $\Delta\Psi$ in PCF *T. brucei*. Further, functional
71 complementation in yeast and mitochondrial swelling experiments suggested that *Tb*MCP11
72 indeed functions as Pi carrier.
73

74 **Material and Methods**

75

76 **Culture and transfection of *Trypanosoma brucei***

77 BSF and PCF *Trypanosoma brucei* strain 449, stably expressing the tetracycline (tet) repressor
78 from the plasmid pHD449, were cultured in standard and HMI-9 medium at 37°C [34] or MEM-
79 PROS medium at 27°C [35] respectively. Media were supplemented with 10% (v/v) fetal calf
80 serum (FCS, Sigma-Aldrich) and 1% penicillin/streptomycin solution (Sigma) and for PCF
81 additionally with 2.5 mg/ml of heme (in 100 mM NaOH). The PCF RNAi cell line EATRO 1125
82 T7T [36], was cultured in semi-defined medium (SDM-79) [37] with 10 µg/ml G418 and 25
83 µg/ml hygromycin. For the experiments described in this paper cells were transfected with
84 different plasmids and clonal cell lines were selected using antibiotics according to the
85 previously published protocol [38].

86

87 **Phylogenetic reconstruction and sequence analysis**

88 Multiple sequence alignments were obtained using ClustalO (www.ebi.ac.uk; Chenna et al.,
89 2003).
90 Phylogenetic reconstruction was performed using the "Phylogeny.fr" software available at
91 http://www.phylogeny.fr. Multiple sequence alignments were obtained using MUSCLE and
92 automatically curated using Gblocks. Maximum likelihood tree was constructed using PhyML
93 and visualized using TreeDyn. Statistical test for branch support was assessed by bootstrap re-
94 sampling analysis generating 100 reiterated data sets. The resulting bootstrap values, expressed
95 as percentage, were added manually to each node. Only bootstrap values above 50% are shown.

96

97 ***Tb*MCP11 N-term peptide antibody**

98 Peptide synthesis and animal immunization were performed by EZBiolab (USA). The
99 synthesized N-terminal peptide 'KNKTWDARYANPD' (amino acid residues 4-16 of
100 *Tb*MCP11) was coupled to keyhole limpet hemocyanin (KLH) and used for the immunization
101 of two rabbits. For western blot the *Tb*MCP11 antibody was used in a 1:5000 dilution.
102

103 **Generation of *T. brucei Tb*MCP11 overexpression cell line**

104 The open reading frame of *Tb*MCP11, i.e. *Tb*927.9.10310, was cloned via *Hind*III/*Bam*HI into
105 the expression vectors pHD 1701 bearing an N-terminal 2x-myc tag [15] . Following sequencing,
106 comparison of the cloned *TbMCP11* sequence from *T. brucei* Lister 427 with the sequence of
107 the corresponding locus *Tb*927.9.10310 in the genome sequence database of *T. brucei* strain 927
108 (available at http://www.genedb.org) revealed only a few sequence differences at the DNA level
109 but none in the predicted amino acid sequence. The resulting plasmid was linearized using *NotI*
110 and transfected into PCF and BSF *T. brucei* strain 449, constitutively expressing the tet-repressor
111 (*TETR BLE*) [39]. Resistant clones were selected using hygromycin (25 µg/ml). Expression of
112 the N-terminal myc-tagged *Tb*MCP11 (*Tb*MCP11-nmyc^{ti}) was induced by the addition of
113 tetracycline (0.5µg/ml) and analyzed by western blotting using a commercial anti-myc antibody
114 (Roche Applied Science). The genotype of the resulting cell line is *TbMCP11*/*TbMCP11* Tetr
115 *BLE TbMCP11-nmyc^{ti} HYG*, which will be further referred to in this paper as *Tb*MCP11-nmyc^{ti}.
116

117 **Construction of the *Tb*MCP11 double-knockout**

118 BSF449 and PCF449 cell lines were used as starting point for the generation of the knockout
119 cell line Δ*Tb*MCP11 (PCF and BSF) respectively. In both cell lines, the two natural *TbMCP11*
120 alleles were deleted from the genome by successive replacement with the neomycin (NEO) and
121 blasticidine (BSD) antibiotic resistance cassettes. The flanking 5'-untranslated region (5'-UTR)
122 and 3'-untranslated regions (3'-UTR) of *TbMCP11* were used as target sequences for

123 homologous recombination. The construction of the knockout cell lines was performed as
124 described previously [18,40–42]. The successful depletion of *Tb*MCP11 was confirmed by
125 western blot analysis.
126
127 **Generation of the *TbMCP11* RNA interference (RNAi) cell line**
128 The EATRO 1125 T7T cell line was used for the generation of the RNAi cell line. Sense and
129 antisense sequence fragments of *Tb*MCP11 were PCR amplified and cloned into the pLEW100
130 vector using restriction enzymes sites according to a previously published protocol [36]. The
131 final construct was used to transfect PCF EATRO 1125 T7T. The cells were selected using 50
132 µg/ml phleomycin. The RNAi of *TbMCP11* was induced by the addition of tetracycline (0.5
133 µg/ml) and the depletion of *TbMCP11* confirmed by reverse transcription PCR (RT-PCR)
134 (Qiagen) and western blot analysis.
135
136 **RNA isolation and Northern blotting**
137 Total RNA was isolated from *T. brucei* using TriFast (PeqLab Biotechnology GmbH). Total
138 RNA (10 µg) was separated by denaturing (formaldehyde) agarose gel electrophoresis and
139 blotted onto Hybond-N membrane (GE Healthcare). Blots were pre-hybridized in hybridization
140 solution (5xSSC, 5xDenhardt´s reagent and 0.5% w/v SDS) for 1h at 65°C and probed overnight
141 at 65°C using a [^{32}P]-dCTP-labelled *TbMCP11* probe. Blots were washed at 65°C in
142 subsequently 1x SSC (0.15 M NaCl, 0.015 M sodium citrate) supplemented with 0.1% w/v SDS,
143 and 0.1xSSC supplemented with 0.1% w/v SDS, followed by final exposure to X-ray film
144 (Kodak).
145
146 **Western blot analysis**
147 For each lane, 2×10^6 trypanosomes were pelleted and resuspended in SDS-containing Laemmli

148 buffer. Proteins were denatured for 5 min at 95°C, separated on a denaturing 12% SDS-PAGE,
149 and subsequently transferred to a Hybond-P membrane (GE Healthcare Life Sciences) in transfer
150 buffer (39 mM glycine, 48 mM Tris-base, 20% v/v methanol, pH 8.3) for 1 h at 100 V. The
151 membrane was blocked 30 min at room temperature in Tris–buffered saline (TBS) containing
152 0.1% (v/v) Tween 20 (TBS-T) supplemented with 7.5% (w/v) non-fat dry milk, and subsequently
153 incubated for 1 h in TBS-T containing 7.5% milk and the primary antibody. The membrane was
154 then washed in TBS-T, followed by incubation for 45 min at room temperature with the
155 respective secondary antibody (GE Healthcare Life Sciences). Finally, the membrane was
156 extensively washed in TBS-T, processed according to the manufacturer's protocol of the ECL
157 detection kit (GE Healthcare Life Sciences), and exposed to ECL-film (GE Health Care Life
158 Sciences).
159
160 **Growth analysis**
161 Procyclic *Tb*MCP11 RNAi cell lines and BSF *Tb*MCP11 knock out cell lines were diluted to a
162 density of 0.25 x 10^6 cells/ml and 0.1 x 10^6 cells/ml, respectively, at the start of the experiment.
163 After induction of the RNAi PCF *Tb*MCP11 RNAi cell line with tetracycline (0.5 µg/ml), cells
164 were diluted every 2 days and counted every 24 h for a period of 8 days. For the BSF *Tb*MCP11
165 knock-out cell line, cells were counted every 24 h for a total of 72 h after induction with
166 tetraycline (0.5 µg/ml). Cell densities were determined using a Neubauer haemocytometer.
167
168 **Immunofluorescence microscopy**
169 Trypanosomes were sedimented by centrifugation at 2,000 x g and resuspended in phosphate-
170 buffered saline (PBS) containing 4% w/v paraformaldehyde. Fixed cells were allowed to settle
171 down and attach to poly-L-lysine-coated microscope slides. Immunofluorescent labelling of
172 trypanosomes with 4,6'-diamidino-2-phenylindole (DAPI), the mitochondrion-specific probe

173 MitoTracker, and the different antibodies (see results) was performed as described previously
174 [41]. Cells were examined using a Leica DM RXA digital de-convolution microscope, and
175 images were recorded using a digital camera (Hamamatsu).
176
177 **Mitochondrial ATP production assay**
178 ATP production assays were performed as described by Schneider *et al.* [8]. Trypanosomes (2 x
179 10^8 cells) were collected by centrifugation at 1,500 x g for 10 min, washed once with SoTE-
180 buffer (20 mM Tris-HCl pH 7.5, 2 mM EDTA, 0.6 M Sorbitol), and resuspended in 1 ml of
181 SoTE-buffer containing 0.008% (w/v) digitonin to permeabilize the plasma membrane. After 5
182 min incubation on ice, the permeabilized cells were centrifuged for 3 min at 8000 x g and 4 °C.
183 The pellet containing the mitochondria-enriched fraction was washed twice with 1 ml SoTE-
184 buffer and resuspended in 0.5 ml of assay buffer (20 mM Tris-HCl pH 7.4, 15 mM KH_2PO_4, 0.6
185 M Sorbitol, 5 mM $MgSO_4$). The assay was set up by mixing 75 µL assay buffer containing 67
186 µMol ADP, 5 mM substrate (i.e. succinate, α-ketoglutarate) and 75 µL assay buffer containing
187 the mitochondria-enriched fraction. In some experiments, the ADP/ATP carrier inhibitor
188 carboxyatractyloside (CATR) (5.2 µM final concentration) or the ATP synthase inhibitor azide
189 (6.8 mM final concentration) were added to the mitochondria containing assay buffer and
190 incubated for 15 min at 25°C prior to the addition of the substrate. Mitochondrial ATP-
191 production was initiated by the addition of substrate and was allowed to take place for 30 min at
192 30°C. The mitochondrial ATP-production was terminated by the addition of 10 µL TE (10 mM
193 Tris-HCl, 1 mM EDTA, pH 8.0), followed by denaturation at 100 °C for 3 min. The formed
194 protein precipitate was removed by centrifugation for 1 min at 1,000 x g. The ATP concentration
195 in the supernatant was measured according to the manufacturer´s protocol of the ATP
196 Bioluminescence Assay Kit CLS II kit (Roche Applied Science) and using the Junior LB9509
197 tube luminometer (Berthold Technologies).

198

199 **Oxygen consumption analysis**

200 Mitochondria-enriched cellular fractions were isolated from 2 x 10^8 *T. brucei* cells using the
201 digitonin permeabilization method as described by Schneider *et al* [8] and resuspended in 0.5 ml
202 assay buffer (20 mM Tris-HCl pH 7.4, 15 mM KH_2PO_4, 0.6 M Sorbitol, 5 mM $MgSO_4$ and 67
203 µMol ADP). Respiration was initiated with the addition of succinate to a final concentration of
204 5 mM. Salicylhydroxamic acid (SHAM) was added to a final concentration of 1 mM to inhibit
205 the *T. brucei* alternative oxidase (TAO) [43]. Azide (6.8 mM), carbonyl cyanide m-chlorophenyl
206 hydrazone (CCCP, 1 mM) and N-ethylmaleimide (NEM, 1.5 mM) were added as inhibitors
207 (control) of mitochondrial respiration. The rate of mitochondrial oxygen consumption was
208 measured at room temperature using a micro dissolved polarigraphic oxygen electrode (Lazar
209 Research Laboratories). Oxygen levels in the sample chamber were calibrated according to the
210 manufacturer's instructions before measurement of the oxygen consumption rates for each
211 sample.

212

213 **Mitochondrial swelling assay**

214 Yeast mitochondria were isolated as described by Daum *et al*. [44]. Mitochondria-enriched
215 fractions were isolated from *Tb*MCP11-depleted (grown without tetracycline for 168 hours) and
216 non-induced (control) *T. brucei* cell lines using the digitonin permeabilization method [8].
217 Phosphate transport was measured using the mitochondrial swelling method as described by
218 Manon and Guerin [45] and as modified by Hamel *et al.* [46]. Briefly, 100 µl of freshly prepared
219 *T. brucei* mitochondria (see Mitochondrial ATP production assay) were resuspended in 1 ml
220 buffer containing 0.2 M potassium phosphate (pH7.4), 38 mM oligomycin and 0.2 mM
221 antimycin. The mitochondrial swelling was induced by addition of 0.04 mM valinomycin and
222 the change in absorbance was monitored in a spectrophotometer at 546 nm.

223

224 **Scanning electron microscopy**

225 *T. brucei* cells were fixed with 2.5% glutaraldehyde in 0.1 M cacodylate buffer, pH 7.2, adhered
226 for 15 min to glass coverslips coated with 0.1% poly-L-lysine, washed in buffer and post-fixed
227 for 30 min with 1% osmium tetroxide in 0.1 M cacodylate buffer, pH 7.2. Thereafter, the samples
228 were dehydrated in acetone, critical point dried and mounted on SEM stubs. The samples were
229 coated with a 20-nm thick gold layer and examined in a Zeiss (Oberkochen, Germany) DSM940
230 scanning electron microscope.

231

232 **Yeast complementation experiment**

233 The open reading frame of *TbMCP11* was PCR amplified and cloned into the yeast expression
234 vector pYPGK18 using the restriction enzyme sites *Sac*I and *Bam*HI [47]. The final construct
235 pYPGK18-*Tb*MCP11 and the empty pYPGK18 expression vector (control) were used to
236 transfect the Mir1/Pic2 double knockout yeast mutant [48] using the lithium acetate/single-
237 stranded carrier DNA method described by Gietz and Wood [49].

238 To investigate complementation, a single colony of the wild type strain 4741, Mir1/Pic2 double
239 knockout yeast mutant and pYPGK18-*Tb*MCP11 or empty pYPGK18 transfected Mir1/Pic2
240 knockout yeast strain were cultured overnight. The cultures were diluted to 20 cells/µl and 5 µl
241 were plated on YPG (1% yeast extract, 2% peptone, 3% glycerol, 2% agar) YPD (1% yeast
242 extract, 2% peptone, 2% dextrose, 2% agar) or YPL (1% yeast extract, 2% peptone, 1% lactate,
243 2% agar) plates and incubated at 30°C for 3 days.

244

245 **Results**

246

247 **The genome of *T. brucei* contains two genes coding for putative phosphate carriers**

248 Using the amino acid sequences of the yeast mitochondrial phosphate (Pi) carriers Mir1 and Pic2
249 as query to BLAST search the *T. brucei* genome database (www.genedb.com) we have
250 previously identified two proteins with high homology to Pi carriers of other eukaryotes namely
251 *Tb*MCP8 (*Tb*927.10.10440, previously *Tb*10.406.0470) and *Tb*MCP11 (*Tb*927.9.10310) [15].
252 Alignment of the *Tb*MCP8 and *Tb*MCP11 amino acid sequences revealed 41% and 53% identity
253 with the human, and 40% and 43% identity with the yeast Pi carriers, respectively. Both
254 trypanosome carriers display the tripartite sequence structure typical for all SLC25A MCF
255 proteins. Each of the three sequence repeats consists of 100 amino acids arranged in two
256 membrane spanning α-helices and contains the conserved signature motif P-X-(DE)-X-
257 (LIVAT)-(KR)-X-(LRH)-(LIVMFY)-(QGAIVM) (Figure 1A and B). Three groups of
258 conserved amino acid residues located within the three repeats, the so-called contact points CPI,
259 CPII and CPIII, were reported to be essential for substrate specific binding and transport (Figure
260 1A and B) [50]. The Pi carriers from *H. sapiens* (SLC25A3) and *S. cerevisiae* (Pic2 and Mir1)
261 all contain "G xxx Q xxx K" at CPI, "K/R Q" at CPII and "M" at CPIII [50]. All three contact
262 points are conserved in *Tb*MCP8 and *Tb*MCP11.

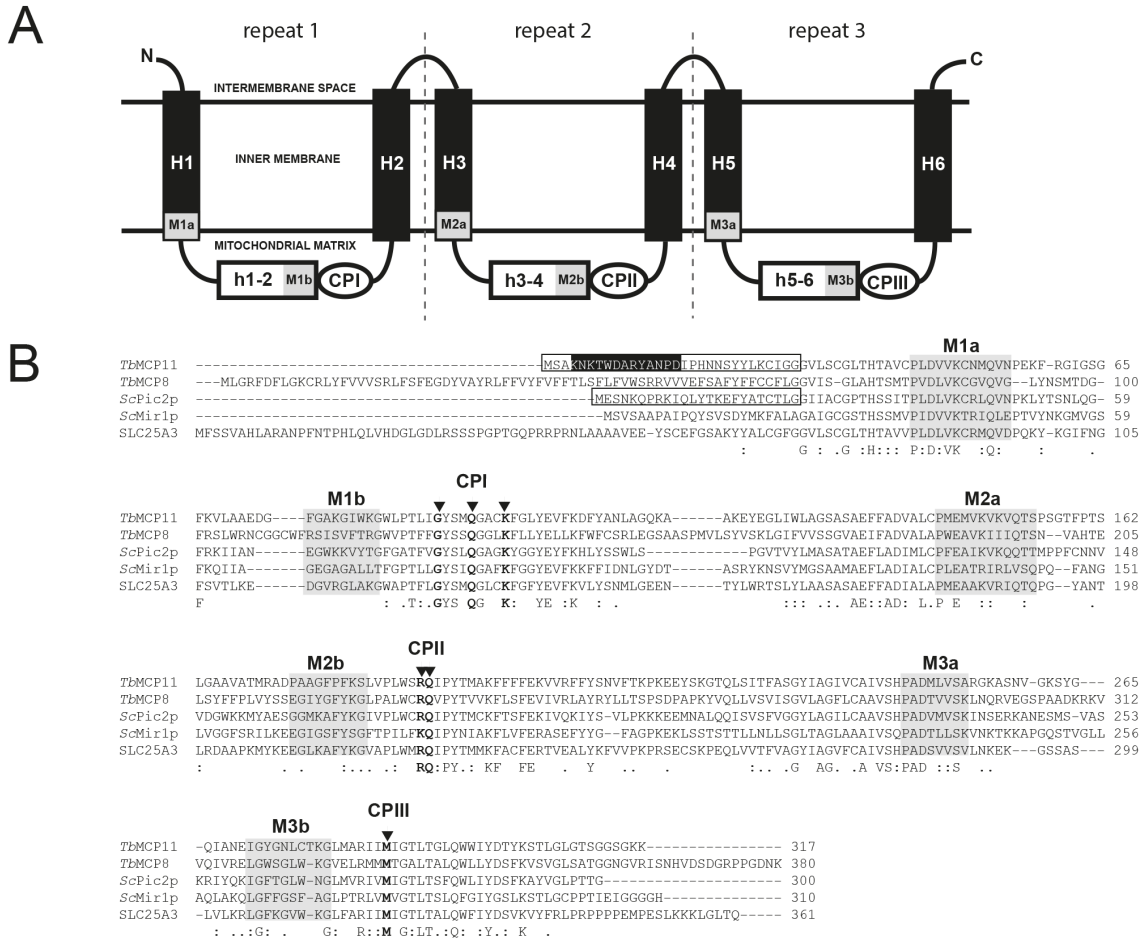

Figure 1. *Tb*MCP11 and *Tb*MCP8 contain sequence motifs and substrate contact point typically found in functionally characterized Pi carriers from other eukaryotes. A: Diagram of MCF protein sequence structure. H1, 2, 3, 4, 5 and 6 are the transmembrane helices, while h1-2, h3-4 and h5-6 are the connecting hydrophilic loops reaching into the mitochondrial matrix. M1a, 2a and 3a are found at the end of each of the odd-numbered transmembrane domains and represent the first part, e.g. Px[D/E]xx[K/R]x[K/R], of the canonical MCF signature. The second part of this MCF signature, e.g. ([D/E]Gx_n[K/R]G), are represented by M1b, 2b and 3b and are located in the middle of each hydrophilic loop. CPI, II and III indicate the three different substrate contact points conserved in most Pi carriers. **B:** Sequence alignment of *Tb*MCP11 and *Tb*MCP8 with *S. cerevisiae* Mir1p (ScMir1p), Pic2p (ScPic2p) and *H. sapiens* SLC25A3 (SLC25A3). The different parts of the MCF signature are boxed in grey. Contact points CPI, II and III are indicated and fully conserved in all analyzed sequences. The N-terminally located,

276 putative mitochondrial targeting sequences of *Tb*MCP11 (amino acids 1-23) and ScPic2p (amino
277 acids 1-17) are boxed. The peptide sequence used for the production of the N-terminal antibody
278 against *Tb*MCP11 is shaded in black.
279
280 Phylogenetic analysis of the putative *T. brucei* Pi carriers *Tb*MCP8 and *Tb*MCP11 and of
281 representative Pi carriers from other eukaryotes resulted in a tree supported by high bootstrap
282 values (Figure S1). As shown previously [51], Pi carriers cluster in clearly distinguishable clades
283 (Figure S1). *Tb*MCP11 clusters into the group of putative Pi carriers from the closely related
284 trypanosomatida *L. infantum*, *T. cruzi* and *T. congolense*, near to the groups of the
285 choanoflagellates and apicomplexa. *Tb*MCP8 however, does not branch into any group. The
286 distinct branching of *Tb*MCP8 and *Tb*MCP11 in the phylogenetic tree is supported by their
287 relatively low sequence similarity (42%) and suggests a divergent evolution of both *Tb*MCPs.
288

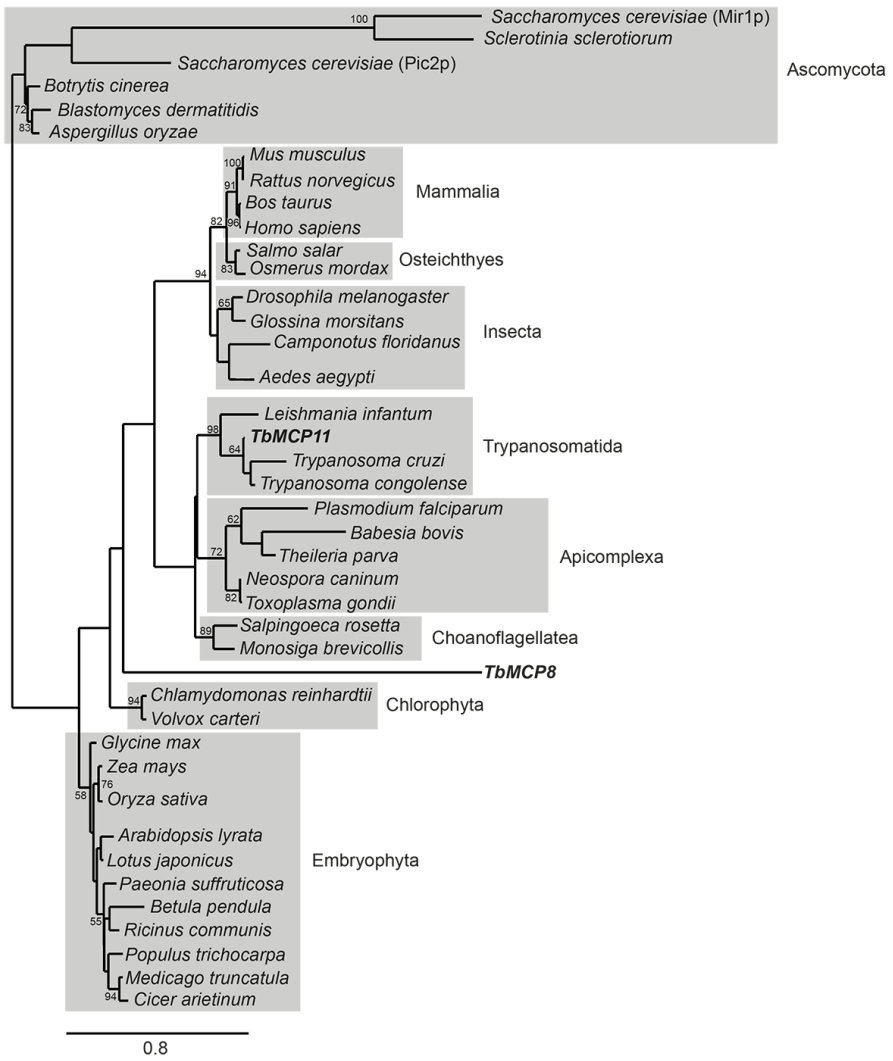

Figure S1. *Tb*MCP11 clusters together with related proteins of other Trypanosomatida, Choanoflagellata and Chromalveolata.

The evolutionary relationship of *Tb*MCP11 with functionally characterized or putative Pi carriers of other species was analyzed using a maximum likelihood tree. The bootstrap consensus tree was obtained after resampling analysis of 100 reiterated data sets. Only significant bootstrap values (≥ 50%) are shown.

The *TbMCP8* gene is not expressed in *T. brucei*

Expression in *T. brucei* is developmentally regulated at the mRNA level for approximately 2% of its genes [52]. Northern blot analysis was performed to assess in which life cycle stage the

300 two putative *T. brucei* Pi carriers are expressed. The results shown in Figure 2 A indicate that
301 the expression of *TbMCP11* is upregulated 3-fold in PCF compared to BSF *T. brucei*. Notably,
302 *TbMCP8* mRNA could not be detected, e.g. was below the detection threshold of the method,
303 for both BSF and PCF *T, brucei* even when using 20 µg of poly-A^+ purified mRNA (not shown).

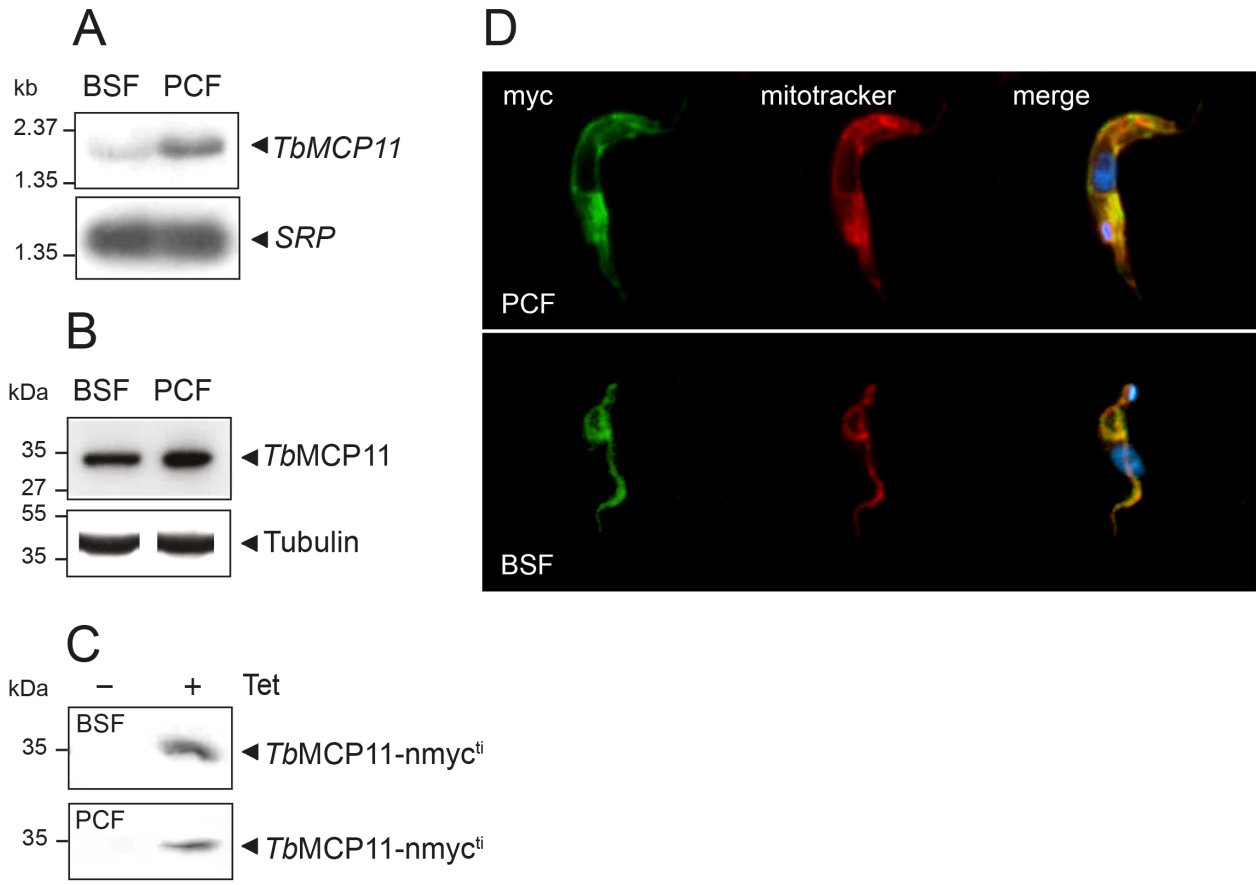

304

305 **Figure 2. *Tb*MCP11 is differentially expressed in BSF and PCF and located exclusively in**
306 **the mitochondrion.**

307 **A:** Northern blot analysis of 10 µg total RNA from BSF and PCF *T. brucei* using a [α^{32}P]-dCTP
308 labelled *TbMCP11* DNA probe. A [α^{32}P]-dCTP labelled signal recognition particle (SRP) probe
309 was used as loading control. **B:** Western blot analysis of protein lysate derived from $2x10^6$ BSF
310 and PCF *T. brucei* using the *Tb*MCP11 antibody in a 1:5000 dilution. An antibody directed
311 against tubulin (dilution 1:1000) was used as loading control. **C:** Western blot analysis of protein
312 lysate derived from $2x10^6$ induced (+ Tet) and non-induced (- Tet) BSF and PCF *T. brucei*

313 expressing N-terminally myc-tagged *Tb*MCP11 (*Tb*MCP11-nmyc^{ti}). The myc-tagged *Tb*MCP11
314 was detected using an antibody against the myc-tag in a 1:1000 dilution. **D:** Immunofluorescence
315 analysis of BSF and PCF *T. brucei* expressing *Tb*MCP11-nmyc^{ti}. An antibody against the myc-
316 tag (green) in a 1:100 dilution was used to localize N-myc-*Tb*MCP11, MitoTracker (red) (0.5
317 µM) was used to visualize mitochondria while DAPI (blue) was used to visualize nuclear and
318 kinetoplast DNA.
319
320 The differential expression of *Tb*MCP11 in BSF and PCF *T. brucei* was confirmed by western
321 blot analysis using an antibody directed against the N-terminus of the protein. In both life cycle
322 stages, a single protein band of approximately 34 kDa (calculated weight of 34.3 kDa) was
323 detected (Figure 2B). Normalization of the western blot using an antibody directed against
324 tubulin shows that the expression of *Tb*MCP11 is 2.5 times upregulated at the protein level in
325 the PCF.
326
327 ***Tb*MCP11 localizes to the mitochondrion of PCF and BSF**
328 The subcellular localization of *Tb*MCP11 was analyzed by immunofluorescence microscopy.
329 We initially used the *Tb*MCP11 peptide-antibody for determining the subcellular localization of
330 *Tb*MCP11 in BSF and PCF *T. brucei*. Unfortunately, staining with this antibody resulted in a
331 high and non-specific background signal in the paraformaldehyde fixed *T. brucei* cells and was
332 found to be not suitable for immunofluorescence microscopy (not shown). Instead, we used BSF
333 and PCF *T. brucei* cell lines expressing N-terminally myc-tagged recombinant versions of
334 *Tb*MCP11 (*Tb*MCP11-nmyc^{ti}) (Figure 2C). The staining of the myc-tag antibody in the
335 *Tb*MCP11-nmyc^{ti} expressing BSF and PCF cell lines and the MitoTracker-labelling superimpose
336 indicating that in both life-cycle stages *Tb*MCP11 localizes to the mitochondrion.
337

338 ***Tb*MCP11 partially complements the function of the yeast Pi carrier**

339 The genome of *S. cerevisiae* contains two isoforms of the mitochondrial Pi carrier, namely Mir1
340 and Pic2. Deletion of both carriers in *S. cerevisiae* (Δ*mir1*Δ*pic2* deletion mutant) abolishes
341 mitochondrial phosphate transport and ATP generation in the yeast [46]. As a consequence,
342 Δ*mir1*Δ*pic2 S. cerevisiae* can only grow on a fermentable carbon source, such as glucose (YPD
343 medium), and not on non-fermentable carbon sources such as glycerol (YPG medium) and
344 lactate (YPL medium) [46,53]. If *Tb*MCP11 facilitates Pi transport across the mitochondrial
345 inner membrane, then the growth defect of the Δ*mir1*Δ*pic2* yeast mutant on non-fermentable
346 carbon sources should be reverted by the heterologous expression of *Tb*MCP11. To this purpose,
347 Δ*mir1*Δ*pic2* was transfected with the yeast expression vector pYPGK18 containing the
348 *Tb*MCP11 open reading frame (pYPGK18-*Tb*MCP11). The empty pYPGK18 vector was used
349 as a negative control. Growth of the resulting *S. cerevisiae* strains was analyzed on YPD, YPG
350 and YPL media, respectively.

351 As expected, the parental *S. cerevisiae* strain BY4741 was able to grow on fermentable (YPD
352 medium) and non-fermentable carbon sources (YPG and YPL media), whereas *S. cerevisiae*
353 Δ*mir1*Δ*pic2::pYPGK18* was only able to grow on YPD medium (Fig. 3A and B).

354

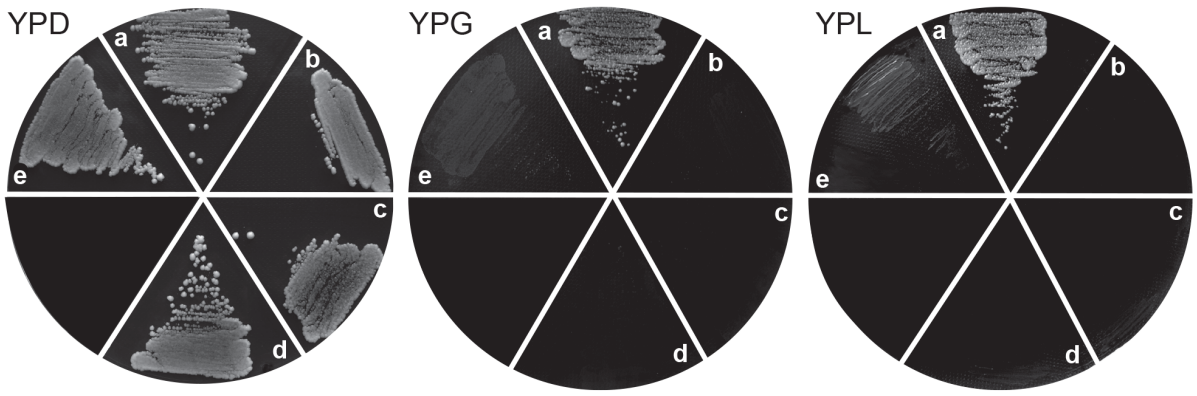

355

356 **Figure 3. *Tb*MCP11 partially complemented the growth defect of the yeast strain**
357 **Δ*mir1*Δ*pic2* on non-fermentable carbon sources.**

358 Yeast cells were grown on either YPD, YPG or YPL medium. For each medium the following
359 strains were plated **a:** the parental 'wildtype' *S. cerevisiae* strain BY4741. **b:** Pi carrier deficient
360 yeast strain Δ*mir1*Δ*pic2*. **c:** Pi carrier deficient yeast strain Δ*mir1*Δ*pic2* transfected with the
361 empty pYPGK18 vector. **d:** Pi carrier deficient yeast strain Δ*mir1*Δ*pic2* transfected with
362 pYPGK18 containing *Tb*MCP11. **e:** Pi carrier deficient yeast strain Δ*mir1*Δ*pic2* transfected
363 with pYPGK18-*TbMCP11-Pic2*^{nterm}.
364
365 Despite the significant amino acid sequence similarity between *Tb*MCP11 and the two yeast Pi
366 carriers Pic2 (62%) and Mir1 (58%), growth of the *S. cerevisiae* strain Δ*mir1*Δ*pic2* on the non-
367 fermentable carbon sources glycerol (YPG) and lactate (YPL) could not be restored to wildtype
368 levels following the heterologous expression of *T. brucei Tb*MCP11 (Figure 3). We previously
369 reported on the partial functional complementation observed for the *T. brucei* MCF carriers
370 *Tb*MCP5 and *Tb*MCP17 upon their expression in the ANC (ATP/ADP) carrier-deficient *S.*
371 *cerevisiae* deletion strain JL1Δ2Δ3u- and the MRS3/4 (iron) carrier deficient *S. cerevisiae*
372 deletion strain GW403, respectively [18,54]. One possible explanation for this could be that *T.*
373 *brucei* MCF proteins are not efficiently sorted to the *S. cerevisiae* mitochondrion due to
374 evolutionary divergence of mitochondrial targeting signal sequences. Sorting problems of
375 heterologously expressed mitochondrial proteins in *S. cerevisae* were previously reported
376 [55,56]. Experiments have shown that for the yeast mitochondrial ATP/ADP carrier ScAnc2 an
377 N-terminal 26 amino acid-long stretch was responsible for a correct and more efficient
378 mitochondrial targeting [56,57]. Indeed, the N-terminus of *Tb*MCP11 differs significantly from
379 the N-termini of both Pic2 and Mir1 (see Figure 1B). To test this possibility, we substituted the
380 first 69 nucleotides (coding for amino acids 1-23) of the *TbMCP11* gene with the first 51
381 nucleotides (coding for amino acids 1-17) of the *ScPic2* gene and cloned the modified ORF
382 (*TbMCP11-Pic2*^{nterm}) into pYPGK18, resulting in pYPGK18-*TbMCP11-Pic2*^{nterm}. After

383 transfection of the *S. cerevisiae* strain Δ*mir1*Δ*pic2* with pYPGK18-*TbMCP11-Pic2*^{nterm} we
384 observed a minimal but clearly increased growth of the *Tb*MCP11-complemented Δ*mir1*Δ*pic2*
385 strain on non-fermentable carbon sources (Figure 3), suggesting a partial complementation by
386 *Tb*MCP11.
387
388 ***Tb*MCP11 is essential for PCF but not BSF *T. brucei* survival**
389 Whether the mitochondrial phosphate carrier *Tb*MCP11 is essential for *T. brucei* viability was
390 assessed by the generation of a targeted gene replacement double-knockout in BSF and by RNA
391 interference in PCF.
392 Using BSF *T. brucei* strain 449, we replaced both *Tb*MCP11 alleles with BSD and NEO
393 antibiotic resistance cassettes to obtain the conventional double knockout cell line
394 Δ*Tb*MCP11::BSD/Δ*Tb*MCP11::NEO. The sequential replacement of both *TbMCP11* alleles was
395 monitored by Southern blot analysis (not shown). The successful depletion of *Tb*MCP11 was
396 further confirmed by western blot analysis (Figure 4B). The deletion of both *Tb*MCP11 alleles
397 in *T. brucei* BSF did not affect growth (Figure 4A) or cell morphology (not shown), suggesting
398 that *Tb*MCP11 is not essential in this life cycle stage.
399
400

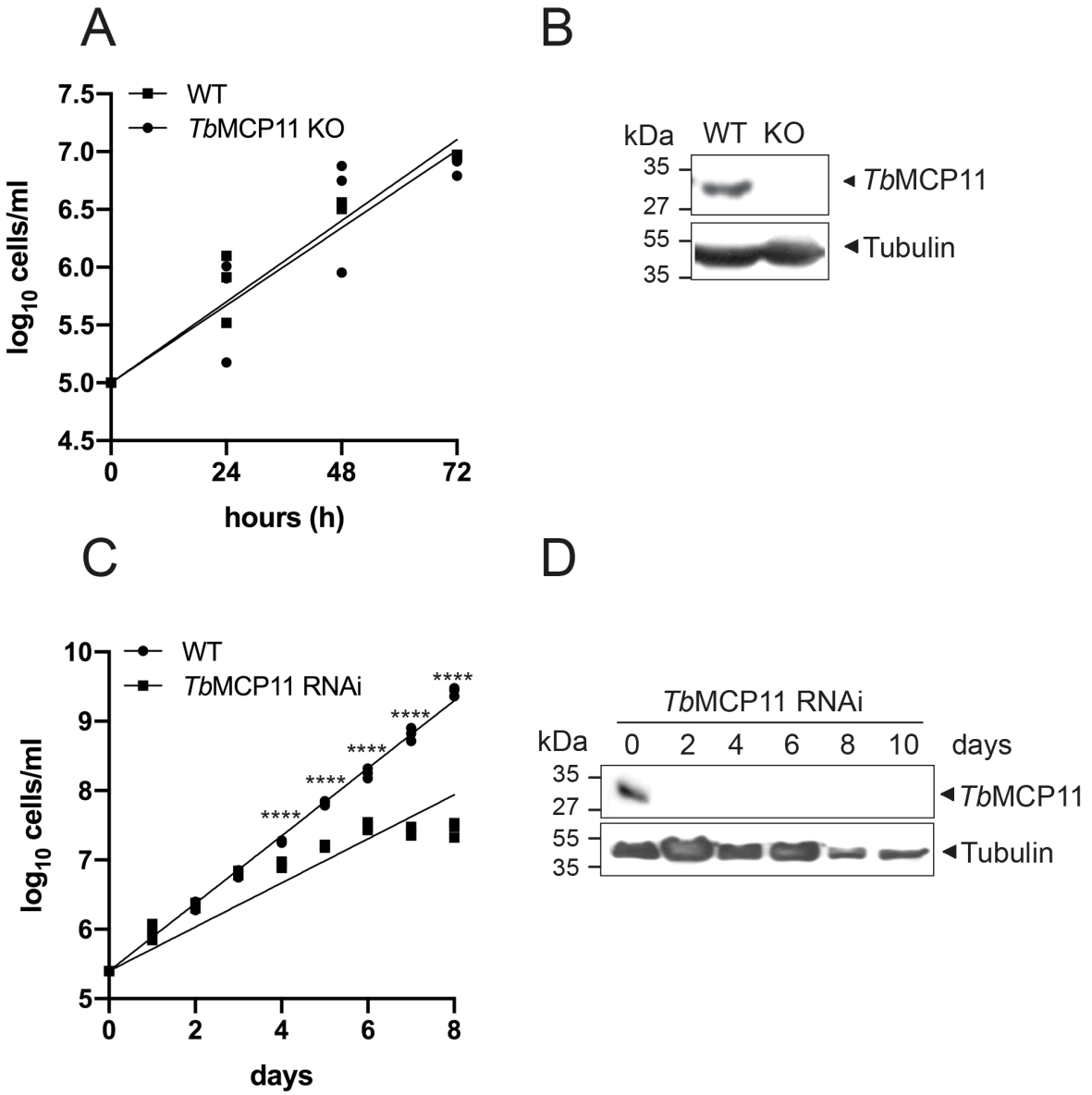

401

402 **Figure 4. *Tb*MCP11 is essential in PCF but not in BSF.**

403 **A:** Cell division analysis of parental ('wild type') *T. brucei* BSF 449 (circles) and the derived
404 Δ*TbMCP11* double-knockout (squares) cell line. **B.** Western blot analysis of cell lysates derived
405 from $2x10^6$ wild type BSF 449 and the Δ*TbMCP11* BSF double-knockout cell line using the
406 raised α*Tb*MCP11 antibody in a 1:5000 dilution. Tubulin was used as loading control. **C:** Cell
407 division analysis of wild type PCF 449 (circles) and tetracycline induced PCF *TbMCP11* RNAi
408 cell line (squares). **D:** Western blot analysis of cell lysates derived from $2x10^6$ tetracycline
409 induced PCF *TbMCP11* RNAi cells using the raised α*Tb*MCP11 antibody in a 1:5000 dilution.

410 Cell samples were taken every 24 h after tetracycline induction. Tubulin was used as loading
411 control. Statistical significance was determined by one-way ANOVA using GraphPad Prism 7:
412 ****$p \leq 0.0001$.
413
414 We next attempted to generate a *Tb*MCP11 double-knockout PCF cell line. Although we were
415 able to generate PCF cell lines lacking only one *TbMCP11* allele (Δ*TbMCP11*::*BSD*/*TbMCP11*),
416 no viable clones could be obtained upon deletion of the second *TbMCP11* allele. This led us to
417 the conclusion that complete depletion of *Tb*MCP11 is lethal for PCF cells, suggesting an
418 essential role for *Tb*MCP11 in this life cycle stage. To confirm this, the RNAi cell line PCF
419 *TbMCP11* RNAi was generated allowing the tetracycline-inducible depletion of *Tb*MCP11.
420 Depletion of *Tb*MCP11 after 2 days until 10 days induction of the RNAi was confirmed by
421 western blot analysis (Figure 4D). In contrast to BSF *T. brucei*, *Tb*MCP11 depleted PCF cells
422 stopped dividing after 5 days of the tetracycline induced RNAi, confirming that *Tb*MCP11 is
423 indeed essential in this life cycle stage (Figure 4C).
424
425 **Pi transport is abolished in *Tb*MCP11-depleted PCF mitochondria**
426 Yeast mitochondria with enabled Pi transport do swell (increase in volume) in the presence of
427 phosphate salt, a property that is lost when the mitochondrial Pi carrier is depleted [24,46] (Table
428 1). Swelling experiments confirmed Pi-dependent swelling also in PCF *T. brucei* mitochondria
429 (Table 1). Analysis of the *Tb*MCP11 RNAi-depleted *T. brucei* mitochondria revealed a major
430 decrease (93%) in mitochondrial swelling, which is similar to decrease observed for Pi-carrier
431 deficient *S. cerevisiae* Δ*mir1*Δ*pic2* mitochondria (Table 1). Heterologous expression of
432 *Tb*MCP11 in the *S. cerevisiae* Δ*mir1*Δ*pic2* strain only partially restored mitochondrial swelling,
433 while the expression of *Tb*MCP11 bearing the 17 N-terminal amino acids of Pic2 fully restored

434 mitochondrial swelling. These results support the hypothesis that *Tb*MCP11 is responsible for
435 mitochondrial Pi import in PCF *T. brucei*.
436

	cell line / strain	ΔAbs_{550nm}	swelling (%)
S. cerevisiae	BY4741 (wildtype)	0.029 ± 0.002	100
	Δmir1/Δpic2	0.002 ± 0.001	7
	Δmir1/Δpic2 + *Tb*MCP11	0.006 ± 0.007	21
	Δmir1/Δpic2 + *Tb*MCP11-Pic2^{nterm}	0.029 ± 0.008	100
PCF *T. brucei*	EATRO1125-T7T	0.149 ± 0.006	100
	*Tb*MCP11^{RNAi} non-induced	0.132 ± 0.008	98
	*Tb*MCP11^{RNAi} induced	0.010 ± 0.007	7

437 438 439 440 441 442 443

444 **Table 1. Mitochondrial swelling in isolated yeast and PCF mitochondria**
445 Mitochondrial swelling experiments were performed in triplicates. The values represent the
446 mean of three independently obtained results and the corresponding standard deviation is
447 indicated.
448

449 **Depletion of *Tb*MCP11 causes aberrant cell-morphology and loss of ΔΨ in PCF *T. brucei***
450 Substantial changes in cell morphology were observed during microscopic examination of
451 *Tb*MCP11-depleted PCF *T. brucei*. In the course of 10 days of *Tb*MCP11 depletion, scanning
452 electron microscopy as well as immunofluorescence analysis revealed several morphological
453 changes compared to wild type cells (Figure 5, Figure 6 and Supplementary Figure S2). The
454 observed morphological changes indicated cytokinesis defects, e.g. multiple cells attached to
455 each other (Figure 5A RNAi day 5 and 10, Figure 6A RNAi day 10, Supplementary Figure S2
456 E) and the presence of single multinucleated cells containing 2-8 nuclei and only one kinetoplast
457 (Figure 6A day 5 and Supplementary Figure S2 B and D). Also, cells were longer and thinner

458 compared to wild type cells (Figure 5 A RNAi day 3, 5 and 10, B and C, Supplementary Figure
459 S2 B). Some cells displayed a fragmented nuclear morphology (Supplementary Figure S2 C).
460

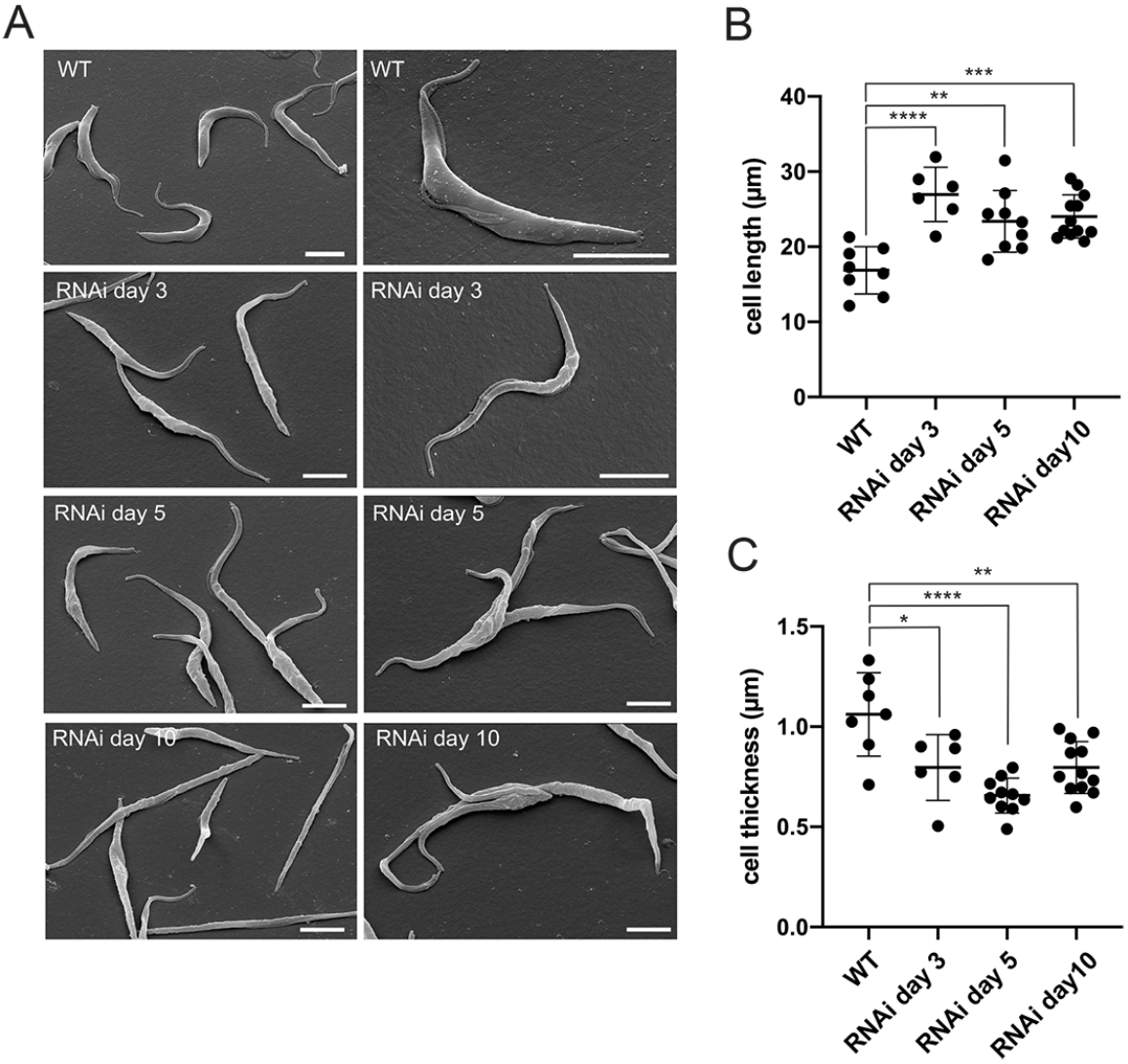

461

462 **Figure 5. *Tb*MCP11 depletion caused abnormal cell morphology and cytokinesis defects in**
463 **PCF *T. brucei*. A:** Scanning electron microscopy (SEM) images from wild type PCF *T. brucei*
464 and *Tb*MCP11 RNAi cell line after 3, 5 and 10 days of RNAi induction using tetracycline. The
465 scale bars represent 5 µm. **B** and **C:** Quantification of cell length (B) and thickness (C) of wild
466 type cells and of the PCF *Tb*MCP11 RNAi cell line after 3, 5 and 10 days of RNAi induction
467 with tetracycline. Measurements were performed using SEM images. Statistical significance was

468 calculated by one-way ANOVA using GraphPad Prism 7: *: $p \leq 0.05$ **: $p \leq 0.01$; ***$p \leq 0.001$;

469 $p \leq 0.0001$.

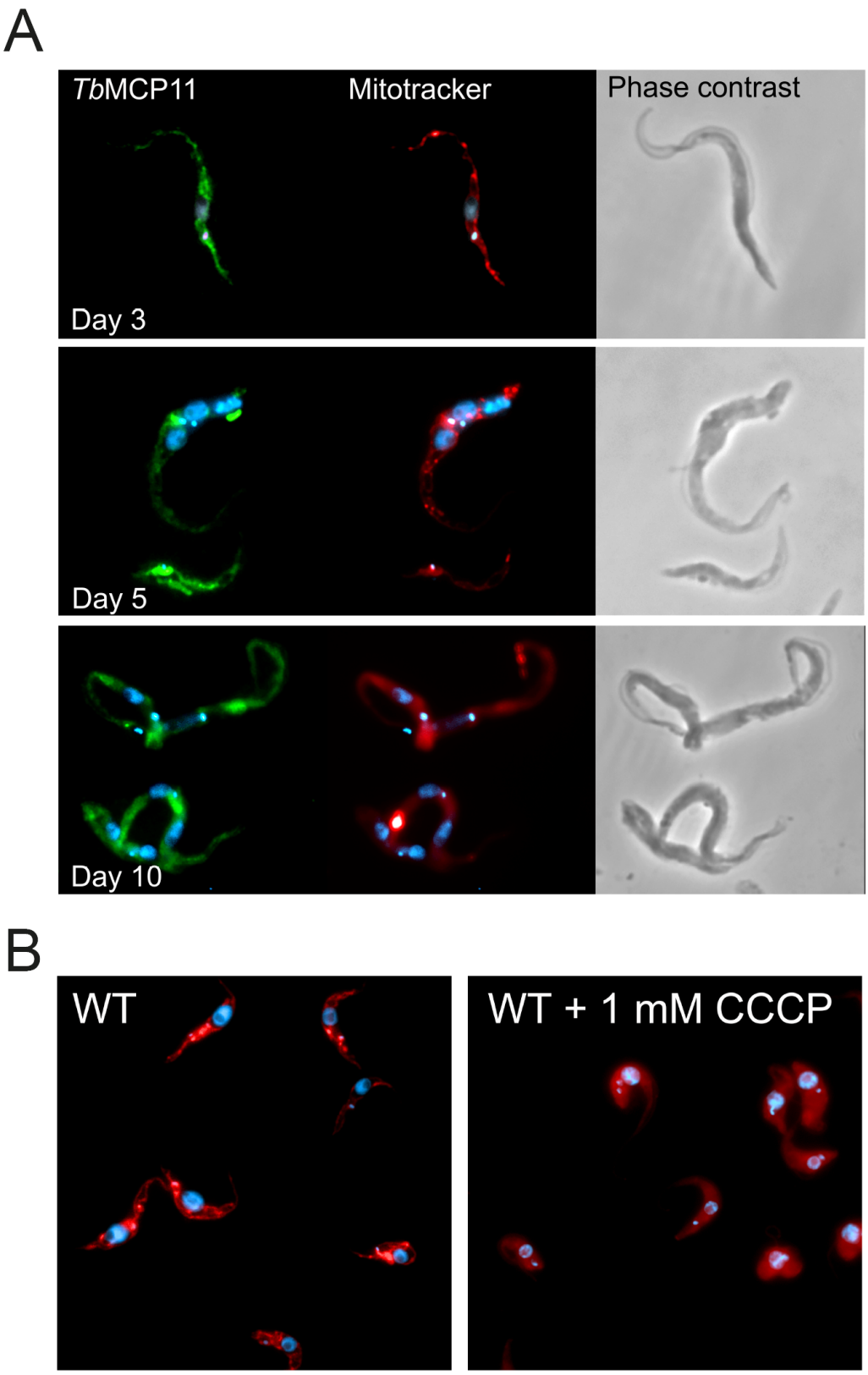

470

471 **Figure 6. *Tb*MCP11 depletion caused loss of mitochondrial morphology and ΔΨ in PCF *T.***
472 ***brucei*. A:** Immunofluorescence analysis of wild type PCF *T. brucei* and the *Tb*MCP11 RNAi
473 cell line after 3, 5 and 10 days of RNAi induction using tetracycline. An antibody against the
474 ADP/ATP carrier *Tb*MCP5 [18] (1:100, green) was used to visualize the mitochondrion.
475 MitoTracker (red) (0.5 μM) was used to visualize the loss of ΔΨ. Nuclei were visualized using
476 DAPI (blue). **B:** Immunofluorescence analysis of wild type PCF and wild type PCF treated with
477 1 mM CCCP to dissipate ΔΨ. Loss of ΔΨ was visualized using MitoTracker (red) (0.5 μM).
478 Nuclei were stained using DAPI (blue).

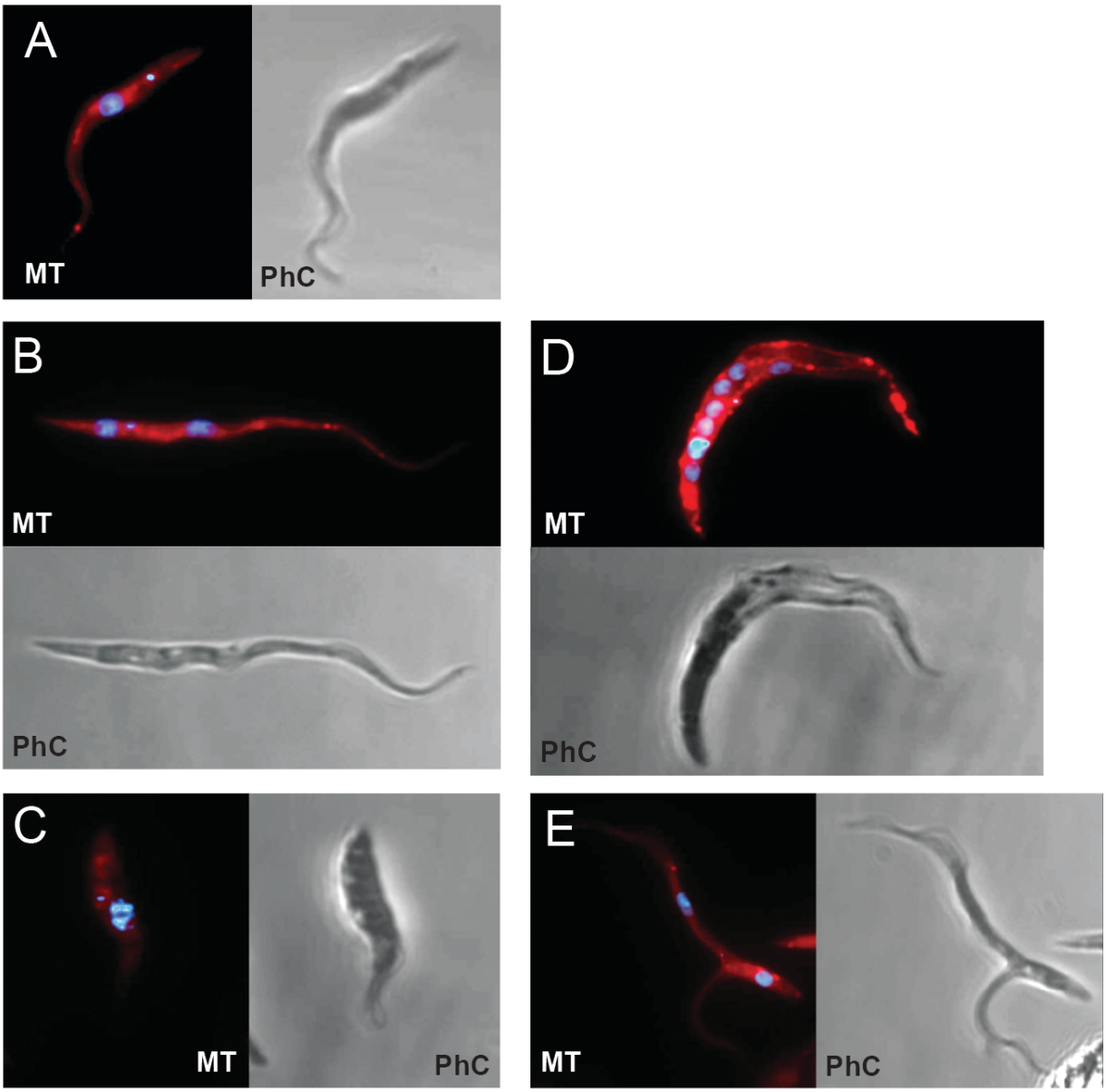

479

480 **Supplementary Figure 2: Aberrant phenotypes after 5-10 days of *Tb*MCP11 depletion.**
481 All cells were stained with MitoTracker (red) (0.5 µM) to visualize the mitochondria and with
482 DAPI (blue) to visualize the nuclei. **A:** Wild type PCF. **B:** *Tb*MCP11 depleted PCF displaying
483 cellular elongation. **C:** *Tb*MCP11 depleted PCF displaying fragmented nucleus. **D:**
484 Multinucleated, giant, *Tb*MCP11 depleted PCF cell. **E:** *Tb*MCP11 depleted PCF displaying
485 incomplete fission. MT: MitoTracker, PhC: Phase contrast.
486
487 We visualized the mitochondrion using an antibody against *Tb*MCP5 [18] and MitoTracker in
488 *Tb*MCP11 depleted PCF at day 3, 5 and 10 after RNAi induction (Figure 6A-C). Until day 3 of
489 induction of the *Tb*MCP11 RNAi the mitochondrion of PCF appeared as a long structure with a
490 number of lateral tubules when marked using either *Tb*MCP5 or MitoTracker (Figure 6A).
491 Instead, after 5 days of induction of the *Tb*MCP11 RNAi, the MitoTracker staining was found
492 to be distributed throughout the cell in what looked like a typical cytoplasm staining (Figure 6B
493 and C). This result hints to the absence of $\Delta\Psi$, which is required for the accumulation of
494 MitoTracker within the mitochondrial matrix [58,59]. The disruption of the $\Delta\Psi$ can be induced
495 by the addition of the ionophore carbonyl cyanide m-chlorophenyl hydrazone (CCCP) [60].
496 Addition of 1 mM CCCP to wild type trypanosomes resulted in the same loss of mitochondria-
497 specific MitoTracker staining as observed for the *Tb*MCP11-depleted cell line (Figure 6C and
498 D).
499
500 **Depletion of *Tb*MCP11 causes loss of mitochondrial ATP production by oxidative**
501 **phosphorylation**
502 ADP and Pi required for the mitochondrial ATP synthesis are provided through the
503 mitochondrial ADP/ATP carrier *Tb*MCP5 [18,19] and the mitochondrial Pi carrier [24,46]
504 respectively. Therefore, ATP synthesis in isolated mitochondria can be used as a method for

505 determining the functionality of the Pi carrier in isolated mitochondria. Using an established
506 mitochondrial ATP production assay [8,42], ATP production was measured for mitochondria
507 isolated from wildtype PCF *T. brucei* and the derived *Tb*MCP11 RNAi cell line using succinate
508 and α-ketoglutarate as substrates. ATP can be generated from α-ketoglutarate by substrate level
509 phosphorylation via succinyl-CoA synthetase and by oxidative phosphorylation via the electron
510 transport chain [29]. From succinate, ATP can only be generated by oxidative phosphorylation
511 [29]. In the non-induced *Tb*MCP11 RNAi cell line the ATP production was 100 pmol/1.5 x 10^7
512 cells for succinate and 220 pmol/1.5 x 10^7 cells for α-ketoglutarate (Figure 7A).
513

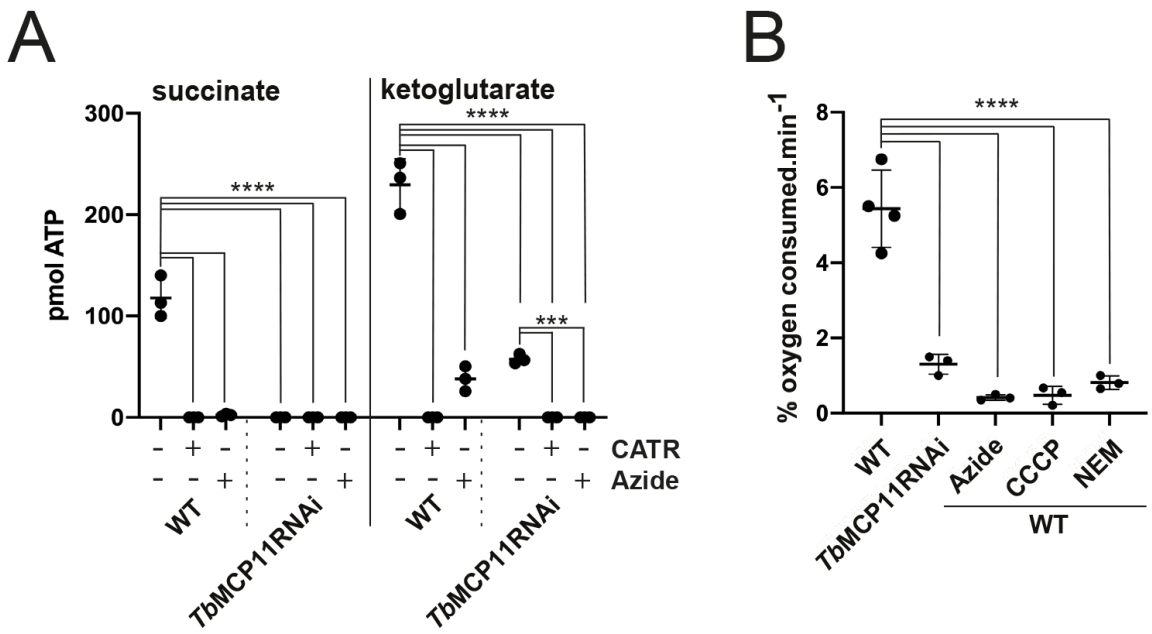

514

515 **Figure 7. Mitochondrial ATP production on succinate and ketoglutarate, as well as oxygen**
516 **consumption, are drastically reduced in PCF *T. brucei* upon depletion of *Tb*MCP11.**
517 Mitochondria were isolated from wildtype PCF *T. brucei* and the derived tetracycline-induced
518 *Tb*MCP11 RNAi cell line. **A:** ATP production in mitochondria isolated from wildtype PCF *T.*
519 *brucei* and the derived tetracycline-induced *Tb*MCP11 RNAi cell line. Mitochondrial ATP
520 production was initiated by addition of 5 mM succinate or 5 mM α-ketoglutarate.

521 Carboxyatractyloside (CATR) (5.2 μM) was added to the mitochondria to inhibit the ATP/ADP
522 carrier, while azide (6.8 mM) was used to inhibit the cytochrome c oxidase. **B:** Oxygen
523 consumption by mitochondria isolated from wildtype PCF *T. brucei* and the derived tetracycline-
524 induced *Tb*MCP11 RNAi cell line. Succinate (5 mM) was added as substrate to initiate oxygen
525 consumption. Azide (6.8 mM), carbonyl cyanide m-chlorophenyl hydrazone (CCCP, 1 mM) and
526 N-ethylmaleimide (NEM, 1.5 mM) were added as controls. Statistical significance was
527 calculated by one-way ANOVA using GraphPad Prism 7: *: $p \leq 0.05$ **: $p \leq 0.01$; ***$p \leq 0.001$;
528 $p \leq 0.0001$
529
530 Addition of carboxyactractiloside (CATR), an inhibitor of the mitochondrial ATP/ADP carrier,
531 abolished mitochondrial ATP production on both substrates due to the lack of import of ADP,
532 indicating that the measured ATP was indeed produced inside the mitochondria (Figure 7A).
533 The addition of azide, an inhibitor of mitochondrial respiration through the blocking of
534 cytochrome c oxidase abolished the production of ATP from succinate and reduced the ATP
535 production from α-ketoglutarate to about 16% (Figure 7A). This is expected since ATP from
536 succinate can only be produced through the respiratory chain, while production of ATP from α-
537 ketoglutarate occurs also over substrate level phosphorylation, which should not be inhibited by
538 azide. The RNAi of *Tb*MCP11 completely abolished ATP production from succinate and
539 reduced the ATP production from α-ketoglutarate to 20% of the ATP production measured in
540 the non-induced *Tb*MCP11 RNAi cell line, which is similar to the reduction observed when azide
541 was added to wild type mitochondria (Figure 7A). The addition of azide combined with the
542 knockdown of *Tb*MCP11 completely abolished the production of ATP from α–ketoglutarate in
543 mitochondria. Overall these results show that depletion of *Tb*MCP11 in PCF *T. brucei* results in
544 the ablation of the mitochondrial $\Delta\Psi$ and that ATP synthesis via oxidative phosphorylation is
545 compromised.

546

547 **Mitochondria depleted of *Tb*MCP11 display drastically reduced oxygen consumption**

548 Mitochondrial respiration and coupled ATP synthesis require the consumption of oxygen, which
549 acts as the terminal electron acceptor. *T. brucei* was previously shown to consume oxygen during
550 mitochondrial respiration [61,62]. We assessed whether isolated mitochondria depleted of
551 *Tb*MCP11 were still consuming oxygen when succinate was provided as a substrate for ATP
552 synthesis (Figure 7B). Oxygen consumption ceased almost completely either when *Tb*MCP11
553 was depleted or when the mitochondrial respiration inhibitors azide, CCCP or NEM were added
554 to wild type mitochondria.

555

556

557 **Discussion**

558

559 Aim of this study was to functionally characterize putative mitochondrial Pi carriers of *T. brucei*.
560 We previously identified *Tb*MCP8 and *Tb*MCP11 as putative mitochondrial Pi carriers in *T.*
561 *brucei* and demonstrated that their predicted protein sequences show significant similarity to the
562 ones of the functionally characterized mitochondrial Pi carriers from both *S. cerevisiae* and
563 humans [15]. However, despite both carriers displaying the expected canonical signature motifs
564 and substrate contact point typically found in mitochondrial Pi carriers (this paper and [15]),
565 *Tb*MCP8 was found to be evolutionary distinct from *Tb*MCP11 and other putative mitochondrial
566 Pi carriers from trypanosomatida (see figure S1). The presence of multiple mitochondrial
567 phosphate carriers is a common feature in eukaryotes [25,63,64]. In mammals two Pi carrier
568 isoforms, e.g. PiC-A and PiC-B, with tissue specific expression can be found [25], while the
569 genome of the plant *Arabidopsis thaliana* encodes three phosphate carriers, e.g. Pic1, Pic2 and
570 PiC3 [21,65,66]. Similar to *Tb*MCP11 and *Tb*MCP8, the two mitochondrial Pi carriers of *S.*
571 *cerevisiae,* e.g. Pic2p and Mir1p, share only 40% sequence homology and phylogenetic analysis
572 indicated that Pic2p is more related to mitochondrial Pi carriers from other eukaryotes than to
573 Mir1p [46]. The presence of different carrier isoforms with low sequence homology, but with
574 conservation of the canonical signature motifs and substrate contact points, suggests rapid
575 evolutionary divergence that facilitates the adaptation to different physiological and
576 environmental conditions while retaining the capacity to transport Pi [26,46]. For example, while
577 Mir1p is constantly expressed in yeast, the steady state expression level of Pic2p was shown to
578 be temperature dependent [46]. In mammals, the two isoforms of PiC A and B are generated by
579 alternative splicing from the same single PiC gene. The expression of PiC A and B appears to
580 be linked to tissue-specific energy demand since PiC A is predominantly found in heart and
581 skeletal muscle, e.g. tissues requiring large amounts of ATP, while PiC B is ubiquitously

582 expressed [26,67]. Northern blot analysis from one of our previous studies showed that *TbMCP8*
583 is not expressed in either BSF or PCF *T. brucei* [15]. Instead, *TbMCP11* is expressed in both
584 replicating *T. brucei* life cycle stages, though at a more prominent level in the PCF, in which
585 depletion of *Tb*MCP11 was shown to be lethal (this paper). These results match previously
586 published transcriptome analyses [68–70] and suggest that *Tb*MCP11 represents the main and
587 only mitochondrial phosphate carrier in PCF, while *Tb*MCP8 might be expressed in one of the
588 non-replicative *T. brucei* life cycle stages or only when the parasite is exposed to specific
589 environmental conditions.
590 Heterologous expression of *Tb*MCP11 partially restored growth of the *S. cerevisiae* Δ*mir1*Δ*pic2*
591 deletion strain on non-fermentable substrates, e.g. glycerol (YPG) and lactate (YPL), and fully
592 restored Pi-dependent mitochondrial swelling, but only when the N-terminus of *Tb*MCP11 was
593 replaced with the one from Pic2 (*Tb*MCP11-Pic2p^{nterm}). This result hints towards an inefficient
594 sorting of the unmodified *T. brucei* Pi carrier to the yeast mitochondrion due to differences in
595 the amino acid sequence at its N-terminus. It was previously shown that the first 26 amino acids
596 of the mitochondrial ADP/ATP-carrier Anc2p were essential for mitochondrial sorting in *S.*
597 *cerevisiae* [57]. However, growth of the *Tb*MCP11-Pic2p^{nterm} expressing Δ*mir1*Δ*pic2* yeast
598 strain on either YPG or YPL medium was never fully restored probably due to other divergences,
599 like for example in protein folding or Pi-transport kinetics, between the *T. brucei* and the yeast
600 Pi-carriers. Interestingly, these divergences did not impact the mitochondrial import of Pi *in*
601 *vitro*, e.g. the import of Pi into isolated mitochondria, suggesting that *in vivo* the *S. cerevisiae* Pi
602 carrier requires some interaction or regulation that cannot be mediated by the heterologous
603 *Tb*MCP11.
604 Our results indicated a decreased mitochondrial membrane potential (ΔΨ) in *Tb*MCP11-depleted
605 *T. brucei* mitochondria. As expected, a disruption of the ATP generation on succinate was
606 observed, which is dependent on the mitochondrial membrane potential and the proton motive

607 force (pmf) [29,71,72]. The mitochondrial depletion of *Tb*MCP11 therefore affected
608 mitochondrial ATP generation not only by abolishing Pi import but also by dissipating the ΔΨ.
609 Loss of the ΔΨ and depletion of mitochondrial Pi following the knockout of PiC were previously
610 observed in *S. cerevisiae* [24]. The authors found that only the addition of Pi to PiC depleted
611 mitochondria could restore the ΔΨ indicating that Pi import was required for sustaining ΔΨ [24].
612 In contrast to succinate, ATP synthesis on α-ketoglutarate can also occur by substrate level
613 phosphorylation via the succinyl CoA synthetase [8,29,30]. Since the RNAi of *Tb*MCP11
614 abolishes the ATP synthesis by oxidative phosphorylation, the persisting ATP synthesis (26%)
615 found on α-ketoglutarate must occur through substrate level phosphorylation using the Pi stored
616 within the mitochondrial matrix. Surprisingly, while azide reduced the ATP synthesis on α-
617 ketoglutarate in wild type mitochondria to similar levels as in the *Tb*MCP11-depleted
618 mitochondria, in combination with the *Tb*MCP11 RNAi it completely abolished ATP
619 production. Taken together, these results strongly indicate that the depletion of *Tb*MCP11 blocks
620 ATP production by oxidative phosphorylation through the dissipation of the ΔΨ. Since the
621 absence of a ΔΨ also disturbs the import and insertion of mitochondrial proteins [24] we
622 speculate that other mitochondrial matrix reactions are affected as well.
623 It was previously shown that patient-derived Pi carrier mutant fibroblasts displayed 50% lower
624 oxygen consumption compared to control fibroblasts due to a defect in the functionality of the
625 electron transport chain [73]. In the *Tb*MCP11-depleted mitochondria oxygen consumption with
626 succinate as substrate was reduced to about 20% compared to wild type mitochondria. This result
627 suggested that 80% of the oxygen consumption was due to the activity of the mitochondrial
628 cytochrome c oxidase present in the respiratory chain complex IV. The oxygen consumption we
629 still observed after *Tb*MCP11 depletion can be attributed to the alternative oxidase (TAO), a
630 cytochrome-independent terminal oxidase located in the mitochondrial membrane of *T. brucei*.
631 TAO transfers electrons derived from the peroxisomal (glycosomal) oxidation of glycerol-3

632 phosphate via ubiquinol to oxygen [43]. The contribution to oxygen consumption by complex
633 IV and TAO within the mitochondria of PCF *T. brucei* corresponds well to the observations
634 published by Horvarth *et al.* [74].
635 Microscopic analysis of the *Tb*MCP11-depleted *T. brucei* cell line further revealed some
636 substantial changes in cell morphology and mitochondrial DNA organization. The presence of
637 multinucleated cells containing only one kinetoplast strongly indicated that *Tb*MCP11 depletion
638 causes, either directly or indirectly, a failure in kinetoplast replication or division. Despite
639 kinetoplast division occurs first, its inhibition does not affect nuclear mitosis [75]. Flagellar
640 division occurs prior the division of the kinetoplast and its dysfunction inhibits cytokinesis but
641 not mitosis [76–78]. In our case flagellar division proceeded normally since the cells in which
642 *Tb*MCP11 was depleted displayed multiple flagella. However, during cell division, the pairing
643 of the daughter kinetoplasts with the daughter flagella and mitochondrial division are a
644 prerequisite to set the morphological axes and serve as checkpoint for cytokinesis [79–82]. This
645 explains why the enlarged *T. brucei* cells found after the depletion of *Tb*MCP11 contain several
646 nuclei but only one kinetoplast.
647 Taken together, our results indicate that *Tb*MCP11 functions as an essential mitochondrial Pi
648 carrier in PCF *T. brucei*. As for other eukaryotic mitochondrial Pi carriers, *Tb*MCP11 is
649 indispensable for mitochondrial ATP synthesis and cell viability. We further speculate that
650 *Tb*MCP11 is required for the maintenance of the mitochondrial membrane potential ($\Delta\Psi$) and
651 that this Pi carrier is involved, either directly or indirectly, in trypanosome cytokinesis.
652
653

654 **References**

655 [1] T. Cavalier-Smith, Eukaryote kingdoms: Seven or nine?, BioSystems. 14 (1981) 461–
656 481. https://doi.org/10.1016/0303-2647(81)90050-2.

657 [2] T. Cavalier-Smith, Higher classification and phylogeny of Euglenozoa, Eur. J. Protistol.
658 56 (2016) 250–276. https://doi.org/10.1016/j.ejop.2016.09.003.

659 [3] Z. Verner, S. Basu, C. Benz, S. Dixit, Eva Dobáková, Drahomíra Faktorová, H. Hashimi,
660 E. Horakova, Z. Huang, Zdeněk Paris, P. Peña-diaz, L. Ridlon, Jiří Týč, D. Wildridge,
661 Alena Zikova, J. Lukeš, Malleable mitochondrion of *Trypanosoma brucei*, Int. Rev. Cell
662 Mol. Biol. 315 (2015) 73–151. https://doi.org/10.1016/bs.ircmb.2014.11.001.

663 [4] S. Bauer, M.T. Morris, Glycosome biogenesis in trypanosomes and the de novo
664 dilemma, PLoS Negl. Trop. Dis. (2017). https://doi.org/10.1371/journal.pntd.0005333.

665 [5] P.A.M. Michels, F. Bringaud, M. Herman, V. Hannaert, Metabolic functions of
666 glycosomes in trypanosomatids, Biochim. Biophys. Acta - Mol. Cell Res. 1763 (2006)
667 1463–1477. https://doi.org/10.1016/j.bbamcr.2006.08.019.

668 [6] P. Peña-Diaz, M. Vancová, C. Resl, M.C. Field, J. Lukeš, A leucine aminopeptidase is
669 involved in kinetoplast DNA segregation in *Trypanosoma brucei*, PLoS Pathog. (2017).
670 https://doi.org/10.1371/journal.ppat.1006310.

671 [7] J. Lukeš, H. Hashimi, Z. Verner, Z. Čičová, The remarkable mitochondrion of
672 trypanosomes and related flagellates, in: 2010. https://doi.org/10.1007/978-3-642-
673 12863-9_10.

674 [8] A. Schneider, D. Bursać, T. Lithgow, The direct route: a simplified pathway for protein
675 import into the mitochondrion of trypanosomes, Trends Cell Biol. 18 (2008) 12–18.
676 https://doi.org/10.1016/j.tcb.2007.09.009.

677 [9] A.K. Panigrahi, Y. Ogata, A. Zíková, A. Anupama, R. a Dalley, P.J. Myler, K.D. Stuart,
678 A comprehensive analysis of *Trypanosoma brucei* mitochondrial proteome, Proteomics.

679 9 (2010) 434–450. https://doi.org/10.1002/pmic.200800477.A.
680 [10] A. Zíková, Z. Verner, A. Nenarokova, P.A.M. Michels, J. Lukeš, A paradigm shift: The
681 mitoproteomes of procyclic and bloodstream *Trypanosoma brucei* are comparably
682 complex, PLoS Pathog. (2017). https://doi.org/10.1371/journal.ppat.1006679.
683 [11] M. Niemann, S. Wiese, J. Mani, A. Chanfon, C. Jackson, C. Meisinger, B. Warscheid,
684 A. Schneider, Mitochondrial outer membrane proteome of *Trypanosoma brucei* reveals
685 novel factors required to maintain mitochondrial morphology, Mol. Cell. Proteomics. 12
686 (2013) 515–528. https://doi.org/10.1074/mcp.M112.023093.
687 [12] J.J. Van Hellemond, F.R. Opperdoes, A.G.M. Tielens, The extraordinary mitochondrion
688 and unusual citric acid cycle in *Trypanosoma brucei*, Biochem. Soc. Trans. 33 (2005)
689 967–971. https://doi.org/10.1042/BST20050967.
690 [13] L. Ernster, G. Schatz, Mitochondria: A historical review, J. Cell Biol. 91 (1981) 227–
691 255. https://doi.org/10.1083/jcb.91.3.227s.
692 [14] E.R.S. Kunji, The role and structure of mitochondrial carriers, FEBS Lett. 564 (2004)
693 239–244. https://doi.org/10.1016/S0014-5793(04)00242-X.
694 [15] C. Colasante, P. Peña Diaz, C. Clayton, F. Voncken, Mitochondrial carrier family
695 inventory of *Trypanosoma brucei brucei*: Identification, expression and subcellular
696 localisation, Mol. Biochem. Parasitol. 167 (2009) 104–117.
697 https://doi.org/10.1016/j.molbiopara.2009.05.004.
698 [16] F. Palmieri, C.L. Pierri, A. De Grassi, A. Nunes-Nesi, A.R. Fernie, Evolution, structure
699 and function of mitochondrial carriers: A review with new insights, Plant J. 66 (2011)
700 161–181. https://doi.org/10.1111/j.1365-313X.2011.04516.x.
701 [17] F. Palmieri, M. Monné, Discoveries, metabolic roles and diseases of mitochondrial
702 carriers: A review, Biochim. Biophys. Acta - Mol. Cell Res. 1863 (2016) 2362–2378.
703 https://doi.org/10.1016/j.bbamcr.2016.03.007.

704 [18] P. Peña-Diaz, L. Pelosi, C. Ebikeme, C. Colasante, F. Gao, F. Bringaud, F. Voncken,
705 Functional characterization of *Tb*MCP5, a conserved and essential ADP/ATP carrier
706 present in the mitochondrion of the human pathogen *Trypanosoma brucei*, J. Biol.
707 Chem. 287 (2012) 41861–41874. https://doi.org/10.1074/jbc.M112.404699.
708 [19] A. Gnipová, K. Šubrtová, B. Panicucci, A. Horváth, J. Lukeš, A. Zíková, The ADP/ATP
709 carrier and its relationship to oxidative phosphorylation in ancestral protist
710 *Trypanosoma brucei*, Eukaryot. Cell. 14 (2015) 297–310.
711 https://doi.org/10.1128/EC.00238-14.
712 [20] R. Krämer, Structural and functional aspects of the phosphate carrier from mitochondria,
713 Kidney Int. 49 (1996) 947–952. https://doi.org/10.1038/ki.1996.133.
714 [21] R. Stappen, R. Krämer, Kinetic mechanism of phosphate/phosphate and phosphate/OH-
715 antiports catalyzed by reconstituted phosphate carrier from beef heart mitochondria, J.
716 Biol. Chem. 269 (1994) 11240–11246.
717 [22] M. Knirsch, M.P. Gawaz, M. Klingenberg, The isolation and reconstitution of the
718 ADP/ATP carrier from wild-type *Saccharomyces cerevisiae* Identification of primarily
719 one type (AAC-2), FEBS Lett. 244 (1989) 427–432. https://doi.org/10.1016/0014-
720 5793(89)80577-0.
721 [23] J.Q. Kwong, J. Davis, C.P. Baines, M.A. Sargent, J. Karch, X. Wang, T. Huang, J.D.
722 Molkentin, Genetic deletion of the mitochondrial phosphate carrier desensitizes the
723 mitochondrial permeability transition pore and causes cardiomyopathy, Cell Death
724 Differ. 21 (2014) 1209–1217. https://doi.org/10.1038/cdd.2014.36.
725 [24] V. Zara, K. Dietmeier, A. Palmisano, A. Vozza, J. Rassow, F. Palmieri, N. Pfanner,
726 Yeast mitochondria lacking the phosphate carrier/p32 are blocked in phosphate transport
727 but can import preproteins after regeneration of a membrane potential., Mol. Cell. Biol.
728 16 (1996) 6524–6531. https://doi.org/10.1128/mcb.16.11.6524.

729 [25] V. Dolce, V. Iacobazzi, F. Palmieri, J.E. Walker, The sequences of human and bovine
730 genes of the phosphate carrier from mitochondria contain evidence of alternatively
731 spliced forms, J. Biol. Chem. 3 (1994) 79–88.
732 [26] G. Fiermonte, V. Dolce, F. Palmieri, Expression in *Escherichia coli*, functional
733 characterization, and tissue distribution of isoforms A and B of the phosphate carrier
734 from bovine mitochondria, J. Biol. Chem. 273 (1998) 22782–22787.
735 https://doi.org/10.1074/jbc.273.35.22782.
736 [27] J. Mayr, F.A. Zimmermann, R. Horvath, H.-C. Schneider, B. Schoser, E. Holinski-
737 Feder, B. Czermin, P. Freisinger, W. Sperl, Mitochondrial phosphate carrier deficiency
738 presenting as (cardio-)myopathy in a family with three affected children, J. Inherit.
739 Metab. Dis. 21 (2011) 803–808. https://doi.org/http://dx.doi.org/10.1007/s10545-011-
740 9371-z.
741 [28] E.J. Bhoj, M. Li, R. Ahrens-Nicklas, L.C. Pyle, J. Wang, V.W. Zhang, C. Clarke, L.J.
742 Wong, N. Sondheimer, C. Ficicioglu, M. Yudkoff, Pathologic variants of the
743 mitochondrial phosphate carrier SLC25A3: Two new patients and expansion of the
744 cardiomyopathy/skeletal myopathy phenotype with and without lactic acidosis, JIMD
745 Rep. 19 (2015) 59–66. https://doi.org/10.1007/8904_2014_364.
746 [29] F. Bringaud, L. Rivière, V. Coustou, Energy metabolism of trypanosomatids:
747 Adaptation to available carbon sources, Mol. Biochem. Parasitol. 149 (2006) 1–9.
748 https://doi.org/10.1016/j.molbiopara.2006.03.017.
749 [30] N. Bochud-Allemann, A. Schneider, Mitochondrial substrate level phosphorylation is
750 essential for growth of procyclic *Trypanosoma brucei*, J. Biol. Chem. 277 (2002)
751 32849–32854. https://doi.org/10.1074/jbc.M205776200.
752 [31] N. Lamour, L. Rivière, V. Coustou, G.H. Coombs, P. Barrett, F. Bringaud, M.P. Barrett,
753 F. Bringaud, Proline metabolism in procyclic *Trypanosoma brucei* is down-regulated in

754 the presence of glucose, J. Biol. Chem. 280 (2005) 11902–11910.
755 https://doi.org/10.1074/jbc.M414274200.
756 [32] T.K. Smith, F. Bringaud, D.P. Nolan, L.M. Figueiredo, Metabolic reprogramming
757 during the *Trypanosoma brucei* life cycle, F1000Research. (2017).
758 https://doi.org/10.12688/f1000research.10342.1.
759 [33] D.J. Creek, M. Mazet, F. Achcar, J. Anderson, D.H. Kim, R. Kamour, P. Morand, Y.
760 Millerioux, M. Biran, E.J. Kerkhoven, A. Chokkathukalam, S.K. Weidt, K.E.V.
761 Burgess, R. Breitling, D.G. Watson, F. Bringaud, M.P. Barrett, Probing the metabolic
762 network in bloodstream-form *Trypanosoma brucei* using untargeted metabolomics with
763 stable isotope labelled glucose, PLoS Pathog. 11 (2015).
764 https://doi.org/10.1371/journal.ppat.1004689.
765 [34] H. Hirumi, K. Hirumi, Continuous cultivation of *Trypanosoma brucei* bloodstream
766 forms in a medium containing a low concentration of serum protein without feeder cell
767 layers, J. Parasitol. 75 (1989) 985–989. https://doi.org/10.2307/3282883.
768 [35] P. Overath, J. Czichos, C. Haas, The effect of citrate/cis-aconitate on oxidative
769 metabolism during transformation of *Trypanosoma brucei*, Eur. J. Biochem. 160 (1986)
770 175–182. https://doi.org/10.1111/j.1432-1033.1986.tb09955.x.
771 [36] E. Wirtz, S. Leal, C. Ochatt, G.A.M. Cross, A tightly regulated inducible expression
772 system for conditional gene knock-outs and dominant-negative genetics in
773 *Trypanosoma brucei*, Mol. Biochem. Parasitol. 99 (1999) 89–101.
774 https://doi.org/10.1016/S0166-6851(99)00002-X.
775 [37] R. Brun, M. Schonenberger, Cultivation and in vitro cloning of procyclic culture forms
776 of *Trypanosoma brucei* in a semi-defined medium. Short communication, Acta Trop. 36
777 (1979) 289–292.
778 [38] S. Biebinger, S. Rettenmaier, J. Flaspohler, C. Hartmann, J. Peña-Diaz, L. Elizabeth

779 Wirtz, H.R. Hotz, J.D. Barry, C. Clayton, The PARP promoter of *Trypanosoma brucei*
780 is developmentally regulated in a chromosomal context, Nucleic Acids Res. 24 (1996)
781 1202–1211. https://doi.org/10.1093/nar/24.7.1202.
782 [39] S. Biebinger, L. Elizabeth Wirtz, P. Lorenz, C. Clayton, Vectors for inducible expression
783 of toxic gene products in bloodstream and procyclic *Trypanosoma brucei*, Mol.
784 Biochem. Parasitol. 85 (1997) 99–112. https://doi.org/10.1016/S0166-6851(96)02815-
785 0.
786 [40] S. Krieger, W. Schwarz, M.R. Ariyanayagam, A.H. Fairlamb, R.L. Krauth-Siegel, C.
787 Clayton, Trypanosomes lacking trypanothione reductase are avirulent and show
788 increased sensitivity to oxidative stress., Mol. Microbiol. 35 (2000) 542–52.
789 [41] F. Voncken, J.J. Van Hellemond, I. Pfisterer, A. Maier, S. Hillmer, C. Clayton,
790 Depletion of GIM5 causes cellular fragility, a decreased glycosome number, and
791 reduced levels of ether-linked phospholipids in trypanosomes, J. Biol. Chem. 278 (2003)
792 35299–35310. https://doi.org/10.1074/jbc.M301811200.
793 [42] C. Colasante, F. Zheng, C. Kemp, F. Voncken, A plant-like mitochondrial carrier family
794 protein facilitates mitochondrial transport of di- and tricarboxylates in *Trypanosoma*
795 *brucei*, Mol. Biochem. Parasitol. 221 (2018) 36–51.
796 https://doi.org/10.1016/j.molbiopara.2018.03.003.
797 [43] M. Chaudhuri, R.D. Ott, G.C. Hill, Trypanosome alternative oxidase: from molecule to
798 function, Trends Parasitol. 22 (2006) 484–491. https://doi.org/10.1016/j.pt.2006.08.007.
799 [44] G. Daum, P.C. Böhni, G. Schatz, Import of proteins into mitochondria. Cytochrome b2
800 and cytochrome c peroxidase are located in the intermembrane space of yeast
801 mitochondria., J. Biol. Chem. 257 (1982) 13028–13033.
802 [45] S. Manon, M. Guerin, Modifications of oxidative phosphorylations in mitochondria
803 isolated from a mutant of *Saccharomyces cerevisiae*. Possible alterations of the

804 phosphate transport, Eur J Biochem. 172 (1988) 205–211.
805 https://doi.org/10.1111/j.1432-1033.1988.tb13874.x.
806 [46] P. Hamel, Y. Saint-Georges, B. De Pinto, N. Lachacinski, N. Altamura, G. Dujardin,
807 Redundancy in the function of mitochondrial phosphate transport in *Saccharomyces*
808 *cerevisiae* and *Arabidopsis thaliana*, Mol. Microbiol. 51 (2004) 307–317.
809 https://doi.org/10.1046/j.1365-2958.2003.03810.x.
810 [47] F.M. Vaz, R.H. Houtkooper, F. Valianpour, P.G. Barth, R.J.A. Wanders, Only one splice
811 variant of the human TAZ gene encodes a functional protein with a role in cardiolipin
812 metabolism, J. Biol. Chem. 278 (2003) 43089–43094.
813 https://doi.org/10.1074/jbc.M305956200.
814 [48] J.A. Mayr, O. Merkel, S.D. Kohlwein, B.R. Gebhardt, H. Böhles, U. Fötschl, J. Koch,
815 M. Jaksch, H. Lochmüller, R. Horváth, P. Freisinger, W. Sperl, Mitochondrial
816 phosphate-carrier deficiency: A novel disorder of oxidative phosphorylation, Am. J.
817 Hum. Genet. 80 (2007) 478–484. https://doi.org/10.1086/511788.
818 [49] R.D. Gietz, R.A. Woods, Transformation of yeast by lithium acetate/single-stranded
819 carrier DNA/polyethylene glycol method, Methods Enzymol. 350 (2002) 87–96.
820 https://doi.org/10.1016/S0076-6879(02)50957-5.
821 [50] E.R.S. Kunji, A.J. Robinson, The conserved substrate binding site of mitochondrial
822 carriers, Biochim. Biophys. Acta - Bioenerg. 1757 (2006) 1237–1248.
823 https://doi.org/10.1016/j.bbabio.2006.03.021.
824 [51] R. Takabatake, S. Hata, M. Taniguchi, H. Kouchi, T. Sugiyama, K. Izui, Isolation and
825 characterization of cDNAs encoding mitochondrial phosphate transporters in soybean,
826 maize, rice, and Arabidopsis, Plant Mol. Biol. 40 (1999) 479–486.
827 https://doi.org/10.1023/A:1006285009435.
828 [52] S. Brems, D.L. Guilbride, D. Gundlesdodjir-Planck, C. Busold, V.D. Luu, M. Schanne,

829 J. Hoheisel, C. Clayton, The transcriptomes of *Trypanosoma brucei* Lister 427 and
830 TREU927 bloodstream and procyclic trypomastigotes, Mol. Biochem. Parasitol. 139
831 (2005) 163–172. https://doi.org/10.1016/j.molbiopara.2004.11.004.
832 [53] R. Takabatake, A.B.M. Siddique, H. Kouchi, K. Izui, S. Hata, Characterization of a
833 *Saccharomyces cerevisiae* gene that encodes a mitochondrial phosphate transporter -
834 Like protein, J. Biochem. 129 (2001) 827–833.
835 https://doi.org/10.1093/oxfordjournals.jbchem.a002926.
836 [54] F. Zheng, C. Colasante, F. Voncken, Characterisation of a mitochondrial iron transporter
837 of the pathogen *Trypanosoma brucei*, Mol. Biochem. Parasitol. 233 (2019) 111221–
838 111234. https://doi.org/10.1016/j.molbiopara.2019.111221.
839 [55] S. Van Wilpe, M.T. Ryan, K. Hill, A.C. Maarse, C. Meisinger, J. Brix, P.J.T. Dekker,
840 M. Moczko, R. Wagner, M. Meijer, B. Gulard, A. Hönlinger, N. Pfanner, Tom22 is a
841 multifunctional organizer of the mitochondrial preprotein translocase, Nature. 23 (1999)
842 1618–1627. https://doi.org/10.1038/46802.
843 [56] K.N. Truscott, K. Brandner, N. Pfanner, Mechanisms of protein import into
844 mitochondria, Curr. Biol. 13 (2003) 326–337. https://doi.org/10.1016/S0960-
845 9822(03)00239-2.
846 [57] G.S. Adrian, M.T. McCammon, D.L. Montgomery, M.G. Douglas, Sequences required
847 for delivery and localization of the ADP/ATP translocator to the mitochondrial inner
848 membrane, Mol. Cell. Biol. 6 (1986) 626–634. https://doi.org/10.1128/mcb.6.2.626.
849 [58] E. Vassella, B. Reuner, B. Yutzy, M. Boshart, Differentiation of African trypanosomes
850 is controlled by a density sensing mechanism which signals cell cycle arrest via the
851 cAMP pathway, J. Cell Sci. 110 (1997) 2661–2667.
852 [59] J.S. Isenberg, Role of the mitochondrial membrane permeability transition (MPT) in
853 rotenone-induced apoptosis in liver cells, Toxicol. Sci. 53 (2000) 340–351.

854 https://doi.org/10.1093/toxsci/53.2.340.
855 [60] R.L. Gallo, J.N. Finkelstein, R.H. Notter, Characterization of the plasma and
856 mitochondrial membrane potentials of alveolar type II cells by the use of ionic probes,
857 BBA - Biomembr. 771 (1984) 217–227. https://doi.org/10.1016/0005-2736(84)90536-
858 4.
859 [61] D.S. Beattie, M.M. Howton, The presence of rotenone-sensitive NADH dehydrogenase
860 in the long slender bloodstream and the procyclic forms of *Trypanosoma brucei brucei*,
861 Eur. J. Biochem. 24 (1996) 888–894. https://doi.org/10.1111/j.1432-
862 1033.1996.00888.x.
863 [62] E.J. Bienen, M. Saric, G. Pollakis, R.W. Grady, A.B. Clarkson, Mitochondrial
864 development in *Trypanosoma brucei brucei* transitional bloodstream forms, Mol.
865 Biochem. Parasitol. 45 (1991) 185–192. https://doi.org/10.1016/0166-6851(91)90085-
866 K.
867 [63] M.J. Runswick, S.J. Powell, P. Nyren, J.E. Walker, Sequence of the bovine
868 mitochondrial phosphate carrier protein: structural relationship to ADP/ATP translocase
869 and the brown fat mitochondria uncoupling protein, EMBO J. 6 (1987) 1367–1373.
870 https://doi.org/10.1002/j.1460-2075.1987.tb02377.x.
871 [64] G.C. Ferreira, R.D. Pratt, P.L. Pedersen, Energy-linked anion transport. Cloning,
872 sequencing, and characterization of a full length cDNA encoding the rat liver
873 mitochondrial proton/phosphate symporter, J. Biol. Chem. 264 (1989) 15628–15633.
874 [65] I. Haferkamp, S. Schmitz-esser, The plant mitochondrial carrier family: functional and
875 evolutionary aspects, 3 (2012) 1–19. https://doi.org/10.3389/fpls.2012.00002.
876 [66] R.D. Pratt, G.C. Ferreira, P.L. Pedersen, Mitochondrial phosphate transport. Import of
877 the H+/P(i) symporter and role of the presequence, J. Biol. Chem. 266 (1991) 1276–
878 1280.

879 [67] J.N.A. De Croos, J.D. McNally, F. Palmieri, K.B. Storey, Upregulation of the
880 mitochondrial phosphate carrier during freezing in the wood frog *Rana sylvatica*:
881 Potential roles of transporters in freeze tolerance, J. Bioenerg. Biomembr. 36 (2004)
882 229–239. https://doi.org/10.1023/B:JOBB.0000031974.35812.c9.
883 [68] J.J. Vasquez, C.C. Hon, J.T. Vanselow, A. Schlosser, T.N. Siegel, Comparative
884 ribosome profiling reveals extensive translational complexity in different *Trypanosoma*
885 *brucei* life cycle stages, Nucleic Acids Res. 42 (2014) 3623–3637.
886 https://doi.org/10.1093/nar/gkt1386.
887 [69] T.N. Siegel, D.R. Hekstra, X. Wang, S. Dewell, G.A.M. Cross, Genome-wide analysis
888 of mRNA abundance in two life-cycle stages of *Trypanosoma brucei* and identification
889 of splicing and polyadenylation sites, Nucleic Acids Res. 38 (2010) 4946–4957.
890 https://doi.org/10.1093/nar/gkq237.
891 [70] A. Naguleswaran, N. Doiron, I. Roditi, RNA-Seq analysis validates the use of culture-
892 derived *Trypanosoma brucei* and provides new markers for mammalian and insect life-
893 cycle stages, BMC Genomics. 19 (2018). https://doi.org/10.1186/s12864-018-4600-6.
894 [71] S. V. Brown, P. Hosking, J. Li, N. Williams, ATP synthase is responsible for
895 maintaining mitochondrial membrane potential in bloodstream form *Trypanosoma*
896 *brucei*, Eukaryot. Cell. 5 (2006) 44–53. https://doi.org/10.1128/EC.5.1.45-53.2006.
897 [72] A. Zíková, A. Schnaufer, R.A. Dalley, A.K. Panigrahi, K.D. Stuart, The F0F1-ATP
898 synthase complex contains novel subunits and is essential for procyclic *Trypanosoma*
899 *brucei*, PLoS Pathog. 5 (2009). https://doi.org/10.1371/journal.ppat.1000436.
900 [73] E.L. Seifert, A. Gál, M.G. Acoba, Q. Li, L. Anderson-Pullinger, T. Golenár, C. Moffat,
901 N. Sondheimer, S.M. Claypool, G. Hajnóczky, Natural and induced mitochondrial
902 phosphate carrier loss: Differential dependence of mitochondrial metabolism and
903 dynamics and cell survival on the extent of depletion, J. Biol. Chem. 291 (2016) 26126–

904 26137. https://doi.org/10.1074/jbc.M116.744714.
905 [74] A. Horváth, E. Horáková, P. Dunajčíková, Z. Verner, E. Pravdová, I. Šlapetová, L.
906 Cuninková, J. Lukeš, Downregulation of the nuclear-encoded subunits of the complexes
907 III and IV disrupts their respective complexes but not complex I in procyclic
908 *Trypanosoma brucei*, Mol. Microbiol. 58 (2005) 116–130.
909 https://doi.org/10.1111/j.1365-2958.2005.04813.x.
910 [75] K. Mensa-Wilmot, B. Hoffman, J. Wiedeman, C. Sullenberger, A. Sharma, Kinetoplast
911 division factors in a trypanosome, Trends Parasitol. 35 (2019) 119–128.
912 https://doi.org/10.1016/j.pt.2018.11.002.
913 [76] K. Gull, S. Alsford, K. Ersfeld, Segregation of minichromosomes in trypanosomes:
914 Implications for mitotic mechanisms, Trends Microbiol. 6 (1998) 319–323.
915 https://doi.org/10.1016/S0966-842X(98)01314-6.
916 [77] A. Selvapandiyan, P. Kumar, J.L. Salisbury, C.C. Wang, H.L. Nakhasi, Role of centrins
917 2 and 3 in organelle segregation and cytokinesis in *Trypanosoma brucei*, PLoS One. 7
918 (2012). https://doi.org/10.1371/journal.pone.0045288.
919 [78] T.C. Hammarton, Cell cycle regulation in *Trypanosoma brucei*, Mol. Biochem.
920 Parasitol. 153 (2007) 1–8. https://doi.org/10.1016/j.molbiopara.2007.01.017.
921 [79] T. Sherwin, K. Gull, The cell division cycle of *Trypanosoma brucei brucei*: timing of
922 event markers and cytoskeletal modulations, Philos. Trans. R. Soc. Lond. B. Biol. Sci.
923 323 (1989) 573–588. https://doi.org/10.1098/rstb.1989.0037.
924 [80] E. Gluenz, M.L. Povelones, P.T. Englund, K. Gull, The kinetoplast duplication cycle in
925 *Trypanosoma brucei* is orchestrated by cytoskeleton-mediated cell morphogenesis, Mol.
926 Cell. Biol. 31 (2011) 1012–1021. https://doi.org/10.1128/mcb.01176-10.
927 [81] R.E. Jensen, P.T. Englund, Network News: The replication of kinetoplast DNA, Annu.
928 Rev. Microbiol. 66 (2012) 473–491. https://doi.org/10.1146/annurev-micro-092611-

929 150057.
930 [82] A. Schneider, T. Ochsenreiter, Failure is not an option - mitochondrial genome
931 segregation in trypanosomes, J. Cell Sci. 131 (2018).
932 https://doi.org/10.1242/jcs.221820.
933

934 **AKNOWLEDGEMENT**

935 This work was funded by the BBSRC, grant number BB/G00448X/1.
936

937 **CONFLICT OF INTEREST**

938 The authors declare that they have no conflicts of interest with the contents of this article.
939

940 **AUTHOR CONTRIBUTION**

941 FG and FV performed the experiments presented in Fig 1, 2, 3, 4 and 7 and Table 1. CC
942 performed the experiments presented in Fig 5, 6 and S1, wrote the manuscript and designed
943 the figures. All authors reviewed the results and corrected the manuscript. The final version of
944 the manuscript was approved by all authors.
945